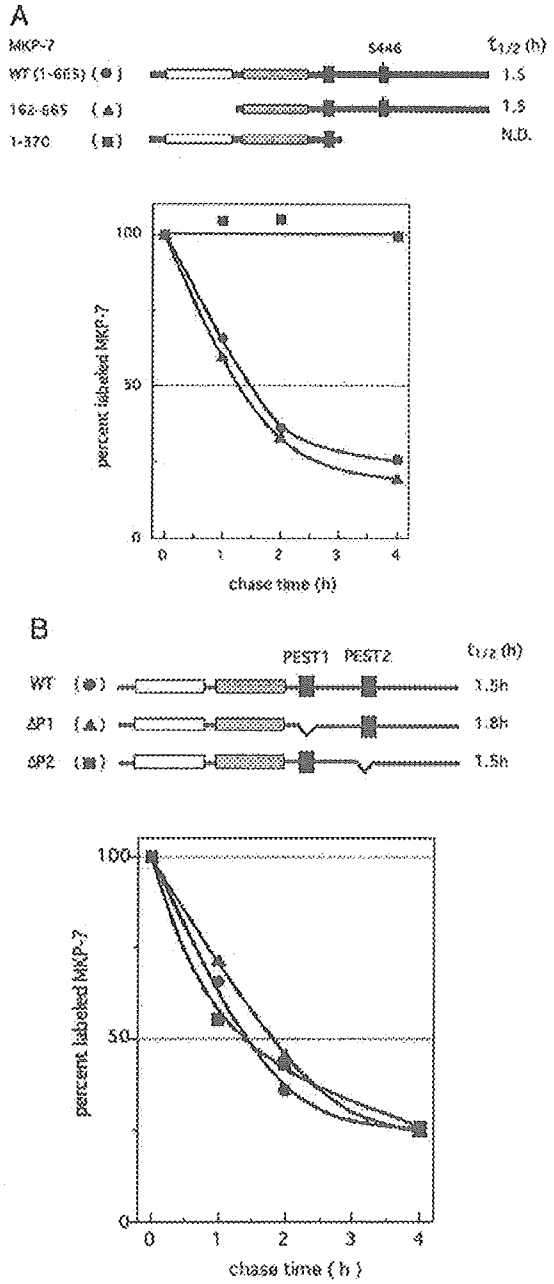

FIG. 3. **COOH-terminal residues but not PEST sequences affect stability of MKP-7.** COS-7 cells (2×10^5/35-mm-diameter plate) were transfected with 1.2 μg of pFLAG-MKP-7WT, pFLAG-MKP-7-(162–665), or pFLAG-MKP-7-(1–370) (*A*) and pFLAG-MKP-7WT, -ΔP1, or -ΔP2 (*B*). At 32 h after transfection, cells were pulsed with [^{35}S]methionine for 1 h and chased for the indicated times. The graph shows the relative intensity of [^{35}S]methionine-labeled MKP-7 mutant proteins. The intensity in labeled cells without chase was defined as 100%. Data shown are the means from three independent experiments. A $t_{1/2}$, obtained from the graph, is presented.

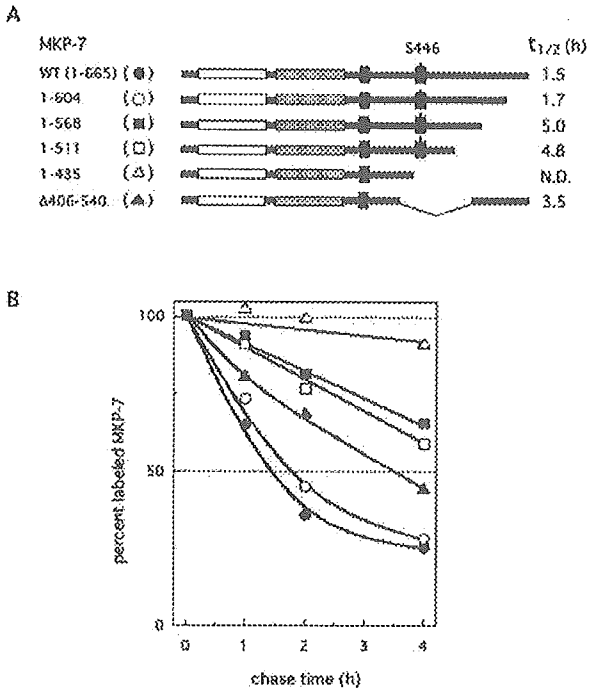

FIG. 4. **Stability of COOH-terminal truncated mutants of MKP-7.** *A*, schematic representation of MKP-7 mutant proteins. *B*, COS-7 cells (2×10^5/35-mm-diameter plate) were transfected with 1.2 μg each of pFLAG-MKP-7WT, pFLAG-MKP-7-(1–604), -(1–568), -(1–511), -(1–435), and -Δ406–540. Thirty-two hours after transfection, cells were pulsed with [^{35}S]methionine for 1 h and chased for the indicated times. The graph shows the relative intensity of [^{35}S]methionine-labeled MKP-7 mutant proteins. The intensity in labeled cells without chase was defined as 100%. Data shown are the means from three independent experiments. A $t_{1/2}$, obtained from the graph, is presented.

protein. In contrast, the half-lives of the upper bands of MKP-7-(371–665) and MKP-7-(390–665) and band of MKP-7-(436–665) were 2.9, 3.2, and 2.8 h, respectively. We demonstrated previously that upon PMA stimulation, Ser-446 of FLAG-MKP-7 is phosphorylated by co-expressed HA-ERK2, resulting in an upward mobility shift of FLAG-MKP-7 seen on SDS-PAGE (10). By analogy, it is possible that the upwardly shifted bands of MKP-7-(371–665) and MKP-7-(390–665) correspond to phosphorylated forms.

Detection of Phosphorylation at Ser-446 in Cells—To detect phosphorylation of Ser-446 in cells, we developed an antibody raised against a peptide containing phosphoserine-446. Cells transfected with FLAG-MKP-7 and HA-ERK2 were stained with this antibody after treatment with or without PMA. No protein was detected by the antibody in cells without PMA-treatment (Fig. 6*A*, *upper panels*). FLAG-MKP-7 was phosphorylated in PMA-treated cells (Fig. 6*A*, *lower panels*), but MKP-7S446A under the same conditions was not (data not shown). These results indicate that the antibody is mono-specific for phospho-Ser-446. Since this antibody did not detect any protein in an immunoblot analysis (data not shown), we conclude that the antibody is suitable only for immunohistological analyses.

To determine whether FLAG-MKP-7-(371–665) and FLAG-MKP-7-(390–665) are phosphorylated in cells even in the absence of HA-ERK2 and without PMA-treatment, COS-7 cells were transfected with pFLAG-MKP-7-(371–665), -(390–665), -(436–665), or -(371–665)S446A and stained with anti-phospho-Ser-446 antibody (Fig. 6*B*) without any stimuli. As shown in Fig. 6*B*, specific interaction with phospho-Ser-446 was confirmed since the antibody does not recognize MKP-7-(371–665)446A (compare *lanes m* and *n*). As shown in Fig. 6*B*, MKP-7-(371–665) was phosphorylated in some cells indicated by arrows but not in others (compare *lanes a* and *b*). Likewise, MKP-7-(390–665) was phosphorylated in some cells as indicated by arrows but not in others (compare *lanes e* and *f*). In

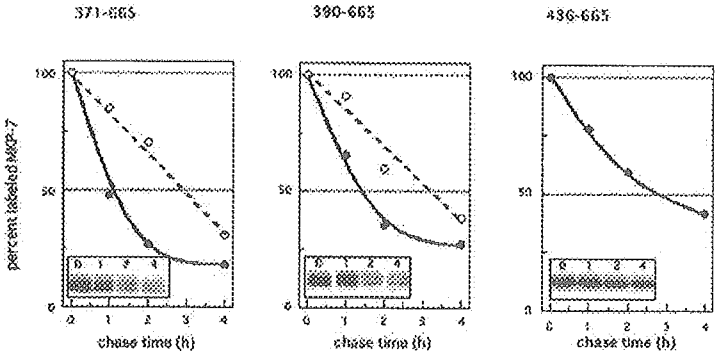

FIG. 5. **Stability of COOH-terminal fragments of MKP-7.** COS-7 cells (2×10^5/35-mm-diameter plate) were transfected with 1.2 μg of pFLAG-MKP-7-(371–665), -(390–665), or -(436–665). Thirty-two hours after transfection, cells were pulsed with [^{35}S]methionine for 1 h and chased for the indicated times. The levels of [^{35}S]methionine-labeled MKP-7 mutant proteins were monitored by autoradiography as shown in *insets*. The graph shows the relative intensity of [^{35}S]methionine-labeled MKP-7 mutant proteins. The intensity in labeled cells without chase was defined as 100%. Data shown are the means from three independent experiments.

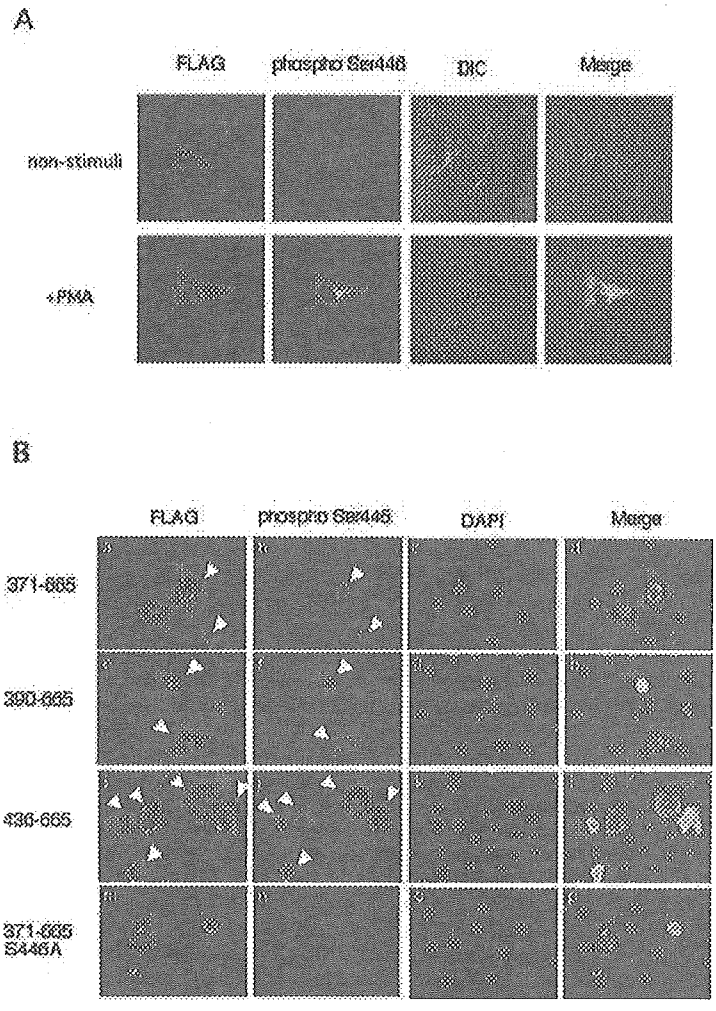

FIG. 6. **Detection of phospho-Ser-446 in the COOH-terminal fragments.** *A*, 36 h after transfection with pFLAG-MKP-7, HeLa cells were cultured without or with 5 ng/ml PMA for 15 min. FLAG-MKP-7 was detected by immunofluorescence using an anti-FLAG rabbit antibody with AlexaFlour-546-conjugated goat anti-rabbit secondary antibody (*red*). Phospho-Ser-446 was detected by immunofluorescence using an anti-phospho-Ser-446 mouse antibody with AlexaFluor-488 conjugated goat anti-mouse secondary antibody (*green*). Cell structure was examined by differential interference contrast (*DIC*). *B*, COS-7 cells transfected with MKP-7-(371–665) (*panels a–d*), -(390–665) (*panels e–h*), -(436–665) (*panels i–l*), or -(371–665)S446A (*panels m–p*) were cultured for 36 h. FLAG-MKP-7 was detected by immunofluorescence using an anti-FLAG rabbit antibody with AlexaFluor-488-conjugated goat anti-rabbit secondary antibody (*panels a*, *e*, *i*, and *m*). Phospho-Ser-446 was detected by immunofluorescence using an anti-phospho-Ser-446 mouse antibody with AlexaFluor-546-conjugated goat anti-mouse secondary antibody (*panels b*, *f*, *j*, and *n*). Nuclei were stained with DAPI (*panels c*, *g*, *k*, and *o*). Cells in which FLAG-MKP-7 is phosphorylated are indicated by *arrows*.

contrast, MKP-7-(436–665) was phosphorylated in almost all transfected cells (compare *lanes i* and *j*). These strongly suggested that the upper bands of MKP-7-(371–665) and MKP-7-(390–665) and the single band of MKP-7-(436–665) seen in Fig. 5 are phosphorylated forms. Since the half-lives of these bands are longer than those of the lower bands of MKP-7-(371–665) and MKP-7-(390–665), it is likely that phosphorylation at Ser-446 stabilizes the CTS fragment. It is significant that expressed COOH-terminal fragments can be phosphorylated even in the absence of HA-ERK2 without PMA stimuli. We showed previously that HA-JNK1 can phosphorylate Ser-446 in a MKP-7CS mutant that lacks JNK phosphatase activity (10). Phosphorylation of the COOH-terminal fragment may be catalyzed not only by endogenous ERK but by endogenous JNK in cells.

Phosphorylation on Ser-446 Stabilizes MKP-7—To confirm that phosphorylation at Ser-446 of the CTS confers stability, the half-lives of MKP-7-(371–665)S446A and -(371–665)-S446D, which are nonphosphorylatable and phosphorylation-mimicking mutants, respectively, were analyzed (Fig. 7, *left*

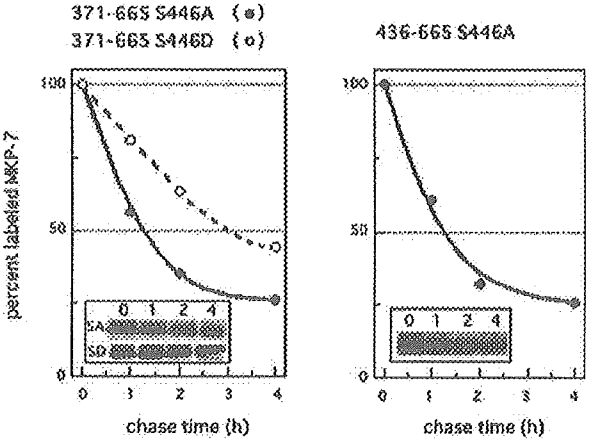

FIG. 7. **Effect of SA and SD mutations on stability of the COOH-terminal fragments.** COS-7 cells (2×10^5/35-mm-diameter plate) were transfected with 1.2 μg of pFLAG-MKP-7-(371–665)S446A, -(371–665)S446D, or -(436–665)S446A. 32 h after transfection, cells were pulsed with [^{35}S]methionine for 1 h and chased for the indicated times. The levels of [^{35}S]methionine-labeled MKP-7 were monitored on autoradiography as shown in the *insets*. The graph shows the relative intensity of [^{35}S]methionine-labeled MKP-7. The intensity in labeled cells without chase was defined as 100%. Data shown are the means from three independent experiments.

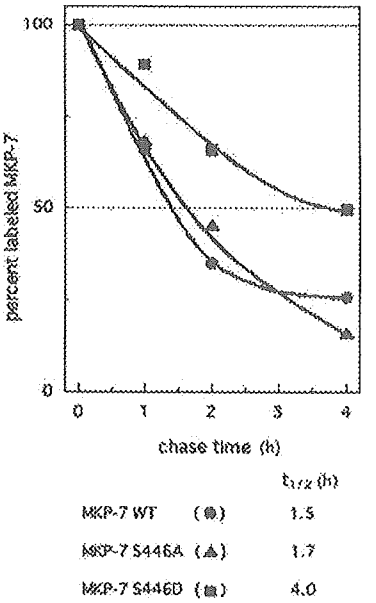

FIG. 8. **A phosphomimicking mutant of MKP-7 has a longer half-life than phosphodefficient MKP-7.** COS-7 cells (2×10^5/35-mm-diameter plate) were transfected with 1.2 μg of pFLAG-MKP-7WT, -S446A, or -S446D. 32 h after transfection, cells were pulsed with [^{35}S]methionine for 1 h and chased for the indicated times. The levels of [^{35}S]methionine-labeled proteins were monitored by autoradiography. The graph shows the relative intensity of [^{35}S]methionine-labeled MKP-7 mutant proteins. The intensity in labeled cells without chase was defined as 100%. Data shown are the means from three independent experiments.

panel). The half-lives of MKP-7-(371–665)S446A and -S446D were 1.3 and 3.2 h, respectively, which is equivalent to the half-lives of the lower and upper bands of MKP-7-(371–665) (Fig. 5, *left panel*). Furthermore, the half-life of MKP-7-(436–665)S446A was shown to be 1.3 h (Fig. 7, *right panel*), which was shorter than that of MKP-7-(436–665) (Fig. 5, *right panel*). These data suggest that phosphorylation at Ser-446 stabilizes the CTS fragment. We then asked whether this finding applies to wild type MKP-7. The time course of degradation of MKP-7S446D, a phosphorylation mimicking mutant, and MKP-7S446A, a nonphosphorylatable mutant in cells with no stimuli, was analyzed (Fig. 8). The half-life of MKP-7S446D was 4.0 h, and that of MKP-7S446A and the wild type protein was 1.5 h, indicating that phosphorylation of Ser-446 stabilizes MKP-7 protein. These data strongly suggest that phosphorylation of Ser-446 increases the half-life of MKP-7 by regulating the stability of the COOH-terminal region.

DISCUSSION

In this study, we found that MKP-7 is a short-lived protein that is degraded via ubiquitin-mediated proteolysis. Two regions, amino acid residues 463–511 and 569–604, in the carboxyl terminus of MKP-7 were shown to target the protein for degradation. We then asked whether protein degradation is regulated by phosphorylation on Ser-446. Using several deletion mutants, we found that upwardly shifted bands in SDS-PAGE corresponding to phosphorylated forms have longer half-lives than the non-shifted ones. Furthermore, a phosphorylation-mimicking mutant of MKP-7 showed a longer half-life than a phosphorylation-deficient one. These results strongly suggested that phosphorylation of Ser-446 of MKP-7 blocks its rapid degradation. MKP-7 suppresses MAPK activation in the order of selectivity, JNK $\gg$ p38 $>$ ERK. We also determined whether phosphorylation at Ser-446 affects substrate specificity. Replacement of Ser-446 by aspartate or glutamate did not mediate any difference in substrate specificity (data not shown). Therefore, we propose that the physiological importance of phosphorylation at Ser-446 is as follows (Fig. 9). In quiescent cells, MKP-7 is maintained at low levels due to rapid turnover by the ubiquitin-mediated protein degradation path-

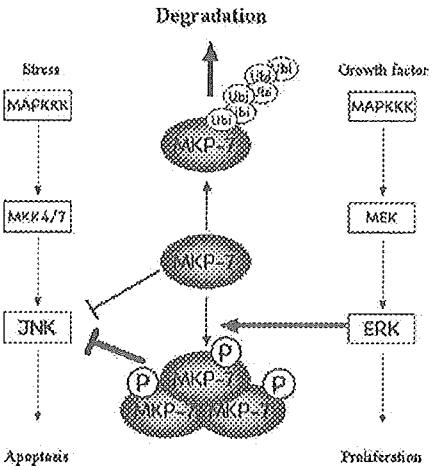

FIG. 9. **Regulation of MKP-7 by phosphorylation on Ser-446.**

way. Upon activation of cells by growth factors, ERK is activated through the MAPKKK/MEK/ERK pathway, and activated ERK can phosphorylate Ser-446 of MKP-7. This phosphorylation does not modify the substrate specificity of MKP-7 but leads to stabilization of the protein. Accumulation-phosphorylated MKP-7 strongly suppress JNK activation.

So far several motifs such as the PEST sequences (16, 17), the cyclin destruction box (22, 23), the KEN destruction box (24), degradation signals of a hydrophobic nature (25, 26), phosphorylation-dependent degradation signals (27), and the myc degron (28) are reported to be required for rapid proteolysis by the ubiquitin-proteasome pathway. Since the identifi-

cation of MKP-7, it has been speculated that MKP-7 is unstable, since it contains two PEST sequences (8). To determine whether these motifs play a role in protein stability, we mutated them (Fig. 3*B*); however, analyses of the mutants showed that their disruption does not increase MKP-7 stability. Instead, regions 1 (463–511) and 2 (569–604) were shown to mediate MKP-7 instability. Regions 1 and 2 may provide binding sites for components of the ubiquitin system, for example by interacting with an E3 ubiquitin ligase. Since deletion of region 1 or 2 independently increases stability, it is possible that such a ligase interacts with both regions 1 and 2. Phosphorylation of Ser-446 may block an E3 ligase from interacting with these regions. On the other hand, our site-directed mutagenesis experiments indicate that the 12 lysine residues present in regions 1 and 2 are not sites for ubiquitination (data not shown). By doing a comparison of the amino acid sequences of regions 1 and 2 with other candidate motifs mentioned above, we found a *RXXL* box, core sequences in the cyclin destruction box (29), at positions 487–490 in region 1. The *RXXL* box is a targeting signal of the anaphase-promoting complex/cyclosome (APC/C), a 1500-kDa complex comprised of many different subunits that serves as the ubiquitin ligase (E3) (30). Identification of targets recognized by regions 1 and 2 is now in progress.

Several reports demonstrated that MKP-1 and MKP-2, which are nuclear MKPs, are short-lived due to ubiquitin-mediated proteolysis (11, 15, 31, 32). Here, we show that MKP-7 is also highly unstable, as is MKP-2 (Fig. 1). We reported previously that MKP-7 is localized exclusively in the cytoplasm, but this localization becomes nuclear following leptomycin B treatment or replacement of leucine by alanine in the nuclear export signal (8). To determine whether localization of MKP-7 affects its degradation, we estimated the half-life of the Leu-to-Ala mutant, which affects nuclear localization. The half-life of the Leu-to-Ala mutant was similar to that of the wild type (data not shown), indicating that the efficiency of MKP-7 degradation is similar in the cytoplasm and in the nucleus.

Previously we mapped MKP-7 to 12p12, an area prone to deletions in acute lymphoblastic leukemia, acute and chronic myeloid leukemia, and myelodysplastic syndrome (8). It has been reported that JNK is constitutively activated in several tumor cell lines and that the transforming action of some oncogene is JNK-dependent (33, 34). Since MKP-7 was identified as a phosphatase specific for JNK, it could also function as a tumor suppressor in cancers through negative regulation of the JNK pathway. Whether the MKP-7 gene is deleted or mutated in tumors from patients is crucially important. Recently it was reported that among 22 leukemia patients analyzed, 17 were hemizygous for MKP-7/DUSP16, but no inactivating mutations could be detected (35), and investigators hypothesized that MKP-7/DUSP16 could be haploinsufficient for tumor suppression. Another group also reported that expression of MKP-7/DUSP16 gene is significantly down-regulated in both clinical tumors and cultured prostate cancer cell lines (36). These data suggest that down-regulation of the MKP-7/DUSP16 gene may be critical for initiation or progression of several tumors. Here we demonstrate that MKP-7 protein levels are regulated by a phosphorylation-dependent, ubiquin-mediated protein degradation pathway. Whether this pathway is impaired in certain cancers remains to be determined.

Recent reports indicate that ERK1/2 activity functions in MKP-1 degradation via the ubiquitin-proteasome pathway. Activation of ERK1/2 induces phosphorylation and reduced degradation of MKP-1 in CCL39 hamster fibroblasts (11) and in *Xenopus* oocytes (14). These observations indicate a control mechanism designed to limit undesirable long term activation of ERK1/2. In contrast, ERK1/2 signaling can trigger degradation of MKP-1 via the ubiquitin-proteasome pathway in CL3 human lung cancer cells treated with Pb(II), a carcinogenic metal (31). In this case, ERK1/2 activation is sustained by stimulating MKP-1 degradation. Data presented here are the first to report that the stability of an MKP other than MKP-1 is regulated by phosphorylation. It is important to note that phosphorylation of MKP-7 by ERK does not affect the ERK pathway positively or negatively but rather affects the JNK pathway. Our results demonstrate that MKP-7 is involved in negative cross-talk between the JNK and ERK pathways and strongly suggest that sustained activation of ERK can result in attenuation of JNK activation through phosphorylation of MKP-7.

Acknowledgements—We thank Dr. Yokosawa for pCI-neo-T7-ubiquitin and pCI-neo-HA-ubiquitin. We also thank E. Yoshida for secretarial assistance.

REFERENCES

1. Chang, L., and Karin, M. (2001) *Nature* **410,** 37–40
2. Wada, T., and Penninger, J. M. (2004) *Oncogene* **23,** 2838–2849
3. Camps, M., Nichols, A., and Arkinstall, S. (2000) *FASEB J.* **14,** 6–16
4. Keyse, S. M., and Ginsburg, M. (1993) *Trends Biochem. Sci.* **18,** 377–378
5. Theodosiou, A., and Ashworth, A. (2002) *Oncogene* **21,** 2387–2397
6. Farooq, A., and Zhou, M.-M. (2004) *Cell. Signal.* **16,** 769–779
7. Alonso, A., Rojas, A., Godzik, A., and Mustelin, T. (2004) *Topics Curr. Genet.* **5,** 333–358
8. Masuda, K., Shima, H., Watanabe, M., and Kikuchi, K. (2001) *J. Biol. Chem.* **276,** 39002–39011
9. Tanoue, T., Yamamoto, T., Maeda, R., and Nishida, E. (2001) *J. Biol. Chem.* **276,** 26629–26639
10. Masuda, K., Shima, H., Katagiri, C., and Kikuchi, K. (2003) *J. Biol. Chem.* **278,** 32448–32456
11. Brondello, J. M., Pouyssegur, J., and McKenzie, F. R. (1999) *Science* **286,** 2514–2517
12. Alonso, A., Rahmouni, S., Williams, S., van Stipdonk, M., Jaroszewski, L., Godzik, A., Abraham, R. T., Schoenberger, S. P., and Mustelin, T. (2003) *Nat. Immunol.* **4,** 44–48
13. Johnson, T. R., Biggs, J. R., Winbourn, S. E., and Kraft, A. S. (2000) *J. Biol. Chem.* **275,** 31755–31762
14. Sohaskey, M. L., and Ferrell, J. E. Jr. (2002) *Mol. Biol. Cell* **13,** 454–468
15. Torres, C., Francis, M. K., Lorenzini, A., Tresini, M., and Cristofalo, V. J. (2003) *Exp. Cell Res.* **290,** 195–206
16. Rechsteiner, M. C., and Rogers, S. W. (1996) *Trends Biochem. Sci.* **21,** 267–271
17. Rechsteiner, M. C. (2004) *Adv. Exp. Med. Biol.* **547,** 49–59
18. Matsuguchi, T., Musikacharoen, T., Johnson, T. R., Kraft, A. S., and Yoshikai, Y. (2001) *Mol. Cell. Biol.* **21,** 6999–7009
19. Sasajima, H., Nakagawa, K., and Yokosawa, H. (2002) *Eur. J. Biochem.* **269,** 3596–3604
20. Yasui, Y., Urano, T., Kawajiri, A., Nagata, K., Tatsuka, M., Saya, H., Furukawa, K., Takahashi, T., Izawa, I., and Inagaki, M. (2004) *J. Biol. Chem.* **279,** 12997–13003
21. Ciechanover, A. (1998) *EMBO J.* **17,** 7151–7160
22. Glotzer, M., Murray, A. W., and Kirschner, M. W. (1991) *Nature* **349,** 132–138
23. King, R. W., Glotzer, M., and Kirschner, M. W. (1996) *Mol. Biol. Cell* **7,** 1343–1357
24. Pfleger, C. M., and Kirschner, M. W. (2000) *Genes Dev.* **14,** 655–665
25. Brodbeck, D., Hill, M. M., and Hemmings, B. A. (2001) *J. Biol. Chem.* **276,** 29550–29558
26. Gilon, T., Chomsky, O., and Kulka, R. G. (2000) *Mol. Cell. Biol.* **20,** 7214–7219
27. Laney, J. D., and Hochstrasser, M. (1999) *Cell* **97,** 427–430
28. Salghetti, S. E., Kim, S. Y., and Tansey, W. P. (1999) *EMBO J.* **18,** 717–726
29. Zur, A., and Brandeis, M. (2002) *EMBO J.* **21,** 4500–4510
30. Peters, J. M., King, R. W., Hoog, C., and Kirschner, M. W. (1996) *Science* **274,** 1199–1201
31. Lin, Y. W., Chuang, S. M., and Yang, J. L. (2003) *J. Biol. Chem.* **278,** 21534–21541
32. Kassel, O., Sancono, A., Kratzschmar, J., Kreft, B., Stassen, M., and Cato, A. C. (2001) *EMBO J.* **20,** 7108–7116
33. Bost, F., McKay, R., Dean, N., and Mercola, D. (1997) *J. Biol. Chem.* **272,** 33422–33429
34. Antonyak, M. A., Moscatello, D. K., and Wong, A. J. (1998) *J. Biol. Chem.* **273,** 2817–2822
35. Hoornaert, I., Marynen, P., Goris, J., Sciot, R., and Baens, M. (2003) *Oncogene* **22,** 7728–7736
36. Kibel, A. S., Huagen, J., Guo, C., Isaacs, W. B., Yan, Y., Pienta, K. J., and Goodfellow, P. J. (2004) *Int. J. Cancer* **109,** 668–672

Am J Physiol Endocrinol Metab 289: E419–E428, 2005.
First published April 12, 2005; doi:10.1152/ajpendo.00512.2004.

Proteomic analysis on insulin signaling in human hematopoietic cells: identification of CLIC1 and SRp20 as novel downstream effectors of insulin

Kumiko Saeki,[1,*] Etsuko Yasugi,[1,*] Emiko Okuma,[1] Samuel N. Breit,[4] Megumi Nakamura,[3] Tosifusa Toda,[3] Yasushi Kaburagi,[2] and Akira Yuo[1]

[1]*Departments of Hematology and* [2]*Metabolic Disorder, Research Institute, International Medical Center of Japan;* [3]*Proteomics Collaboration Research Group, Tokyo Metropolitan Institute of Gerontology, Tokyo, Japan; and* [4]*Centre for Immunology, St. Vincent's Hospital, and University of New South Wales, Sydney, Australia*

Submitted 27 October 2004; accepted in final form 11 April 2005

Saeki, Kumiko, Etsuko Yasugi, Emiko Okuma, Samuel N. Breit, Megumi Nakamura, Tosifusa Toda, Yasushi Kaburagi, and Akira Yuo. Proteomic analysis on insulin signaling in human hematopoietic cells: identification of CLIC1 and SRp20 as novel downstream effectors of insulin. *Am J Physiol Endocrinol Metab* 289: E419–E428, 2005. First published April 12, 2005; doi:10.1152/ajpendo.00512.2004.—Insulin/IGF-I-dependent signals play important roles for the regulation of proliferation, differentiation, metabolism, and autophagy in various cells, including hematopoietic cells. Although the early protein kinase activation cascade has been intensively studied, the whole picture of intracellular signaling events has not yet been clarified. To identify novel downstream effectors of insulin-dependent signals in relatively early phases, we performed high-resolution two-dimensional electrophoresis (2-DE)-based proteomic analysis using human hematopoietic cells 1 h after insulin stimulation. We identified SRp20, a splicing factor, and CLIC1, an intracellular chloride ion channel, as novel downstream effectors besides previously reported effectors of Rho-guanine nucleotide dissociation inhibitor 2 and glutathione *S*-transferase-pi. Reduction in SRp20 was confirmed by one-dimensional Western blotting. Moreover, MG-132, a proteasome inhibitor, prevented this reduction. By contrast, upregulation of CLIC1 was not observed in one-dimensional Western blotting, unlike the 2-DE results. As hydrophilic proteins were predominantly recovered in 2-DE, the discrepancy between the 1-DE and 2-DE results may indicate a certain qualitative change of the protein. Indeed, the nuclear localization pattern of CLIC1 was remarkably changed by insulin stimulation. Thus insulin induces the proteasome-dependent degradation of SRp20 as well as the subnuclear relocalization of CLIC1.

HL-60 cells; PDQuest; matrix-assisted laser desorption ionization coupled to time-of-flight mass spectrometry; Mascot

INSULIN AND INSULIN-LIKE GROWTH FACTOR I (IGF-I) are known as important regulators of a variety of biological effects, including growth, development, and metabolism. Moreover, insulin-dependent signals contribute to the regulation of azurophil granule-selective macroautophagy in human hematopoietic cells (16). The molecular mechanisms for the actions of insulin and IGF-I have been intensively studied by various approaches, including gene-targeting animal experiments (1, 8, 14, 22) and molecular cloning techniques (20, 21). Now, the scenario for early intracellular signal transduction including a protein kinase activation cascade is well documented. It has been revealed that common intracellular signaling pathways are working downstream of insulin and IGF-I, including insulin receptor substrates (IRSs) (12) and Shc (17). The IRSs phosphorylate phosphatidylinositol 3-kinase to activate Akt, which transmits signals for proliferation and survival as well as the hematopoietic macroautophagy regulation (16), and the mammalian target of rapamycin and S6 kinase, which transmit signals for growth and translation besides heaptic macroautophagy regulation (2). On the other hand, Shc transmits signals for differentiation in hematopoietic cells (25).

In contrast to the early signal transduction, the picture of the later signaling events remains rather obscure. A large number of still undetermined molecules may be working downstream of the insulin-dependent signals. To obtain the whole picture of the intracellular signaling events downstream of the insulin receptor, comprehensive studies such as transcriptome analysis and proteome analysis may be especially powerful. A transcriptome analysis can illuminate the intracellular signaling events if they require new transcriptions or altered message stabilities. However, changes in protein expression are not always associated with those of the message expression, and vice versa. Thus transcriptome analysis would occasionally bring about false positive and/or false negative results. In this sense, proteome analysis is thought to be a more practical tool. Moreover, proteome analysis has merit in demonstrating protein modification changes such as phosphorylation and acetylation besides the change in net expression amounts. Indeed, studies on proteome analysis have successfully identified the protein molecules associated with metabolic regulation in the liver (3, 7). However, proteome analysis on insulin signaling in hematopoietic cells has not been performed despite the significance of insulin-dependent signals in the hematopoietic system.

For the first time, we performed proteomic analysis using human hematopoietic cells with the high-resolution two-dimensional electrophoresis (2-DE) system. We show that SRp20, a splicing factor, and CLIC1, an intracellular chloride ion channel, are working as novel downstream effectors of insulin signaling. The biological relevance of these events is discussed.

MATERIALS AND METHODS

Cells, growth factors, and inhibitors. HL-60 cells were maintained in RPMI 1640 medium (Life Technologies, Grand Island, NY) supplemented with 10% heat-inactivated fetal calf serum (FCS; JRH Bioscience, Lenexa, KS). For insulin-stimulating experiments, cells

* These authors contributed equally to this work. The order of the authors' names was arbitrarily arranged.

Address for reprint requests and other correspondence: A. Yuo, Dept. of Hematology, Research Institute, International Medical Center of Japan, 1-21-1 Toyama, Shinjuku-ku, Tokyo 162-8655, Japan (e-mail: yuoakira@ri.imcj.go.jp).

The costs of publication of this article were defrayed in part by the payment of page charges. The article must therefore be hereby marked "*advertisement*" in accordance with 18 U.S.C. Section 1734 solely to indicate this fact.

had been previously cultured in serum-free RPMI 1640 medium supplemented with 5 μg/ml human holo-transferrin (Sigma Chemical, St. Louis, MO) for 3 days, and then 5 μg/ml insulin (Sigma) were added. Transferrin was suspended in RPMI 1640 medium, and insulin was solubilized by 1 N hydrochloride. In some experiments, MG-132 (Calbiochem, La Jolla, CA) was added 30 min before insulin stimulation.

Two-dimensional gel electrophoresis with quantitative analyses. Insulin-depleted cells were stimulated by insulin. After a 1-h incubation, stimulated and nonstimulated cells were collected. After a washing with wash buffer (10 mM Tris·HCl buffer, pH 8.0, 5 mM magnesium acetate), 4×10^7 cells were suspended with 7 volumes of lysis buffer containing 2 M thiourea, 7 M urea, 4% (wt/vol) CHAPS, and 1 mM Pefabloc SC PLUS (Roche Diagnostics, Mannheim, Germany). The cell suspensions were kept for 10 min on ice, sonicated intermittently, and centrifuged at 12,000 *g* for 10 min at 4°C, and the supernatant fractions were collected. The protein concentration was determined in the lysis solution with a dye reagent from Amersham Biosciences (Piscataway, NJ), using BSA as a standard. The lysate was alkylated with Ready Prep Reduction-Alkylation Kit (Bio-Rad Laboratories, Hercules, CA). The 120 μg of protein lysate per gel were subjected to two-dimensional gel electrophoresis (2-DE). One-dimensional isoelectric focusing was carried out using Immobiline dry strip (18 cm long, pH 3–10 nonlinear or pH 4–7 linear, Amersham Biosciences) in a horizontal electrophoresis system (Ettan IPGphor, Amersham Biosciences) according to the manufacturer's instructions. After the one-dimensional elecrofocusing, IPG gels were equilibrated with buffer containing 50 mM Tris·HCl (pH 8.8), 6 M urea, 30% (vol/vol) glycerol, 2% (wt/vol) sodium dodecyl sulfate (SDS), 0.01% bromophenol blue, and 0.5% dithiothreitol, followed by alkylation with equilibration buffer containing 4.5% idoacetamide instead of 0.5% dithiothreitol at room temperature for 15 min. The gels were subjected to two-dimensional SDS-PAGE (10% gel). Proteins were visualized in the gels by staining with SYPRO Ruby Protein Gel Stain (Bio-Rad Laboratories) for overnight. The florescence intensity of each protein spot was digitally recorded by FluorImager 595 (Amersham Biosciences) using ImageQuaNT software and the differential protein expression quantitatively analyzed by PDQuest software (Bio-Rad Laboratories). The density of each spot was normalized by that of the smallest β-actin spot. Initially, all of the spots were roughly matched by an automatic program in PDQuest software, which was followed by a more detailed manual matching process to correct inappropriate matching pairs. Three to six independent experiments were performed, and the results were statistically analyzed by Student's *t*-test.

Mass spectrometric analysis. Mass spectrometric analysis was performed according to the method reported by Toda et al. (23), with slight modifications. Briefly, each protein spot in SYPRO Ruby-stained gels was picked by FluoroPhoreStar 3000 (Anatech, Tokyo, Japan). The pieces of gels were dehydrated in 50% acetonitrile and 50% ammonium bicarbonate, next in 100% acetonitrile, and dried. The proteins were digested with 5 μg/ml trypsin (sequencing grade modified trypsin; Promega, Madison, WI) at 30°C. After overnight protein digestion, peptide fragments in the digest were subjected to matrix-assisted laser desorption ionization (MALDI) coupled to a time-of-flight (TOF) (MALDI-TOF) mass spectrometer (AXIMA-CFR; Shimazdu, Kyoto, Japan) for peptide mass fingerprinting (PMF). Protein identification was performed with the Mascot server (Matrix Science, Boston, MA) and Protein Prospector (UCSF Mass Spectrometry Facility, San Francisco, CA). We selected the *Homo sapiens* database of SWISS-PROT and parameters: peptide tolerance ± 0.4 Da and one missed cleavage. Carbamidomethyl modification of cysteine and acetylation of the NH_2-terminal end or lysine and phosphorylation of serine, threonine, or tyrosine were considered. Protein identification was repeated at least once with spots from different gels. Phosphorylated peptides were confirmed by MALDI-TOF-MS in a postsource decay (PSD) mode of AXIMA-CFR and AXIMA-CFRplus (Shimadzu). NH_2-terminal acetylation was determined by MALDI-QIT-TOF-MS in an MS/MS mode (AXIMA-QIT, Shimadzu).

One-dimensional Western blotting. Cells (5×10^5) were lysed with 100 μl of 1× Laemmli's sample buffer and boiled. Ten microliters of this lysate were subjected to SDS-PAGE with 15% gels. The electric transfer onto a polyvinylidene difluoride (PVDF) membrane was carried out with a semidry blotting apparatus (Bio-Rad Laboratories) at 50 mA/cm^2 for 45 min at room temperature using buffer containing 2.25% Tris, 10.8% glycine, and 20% methanol. The first antibody reaction was performed using anti-SRp20 antibody (7B4; Santa Cruz Biotechnology, Santa Cruz, CA), anti-Rho-guanine nucleotide dissociation inhibitor (Rho-GDI) antibody (A-20; Santa Cruz Biotechnology), anti-β-tubulin antibody (H-235; Santa Cruz Biotechnology), a sheep anti-CLIC1 antiserum (25), anti-cyclin D3 antibody (C-16; Santa Cruz Biotechnology), anti-cyclin E antibody (M-20; Santa Cruz Biotechnology), and anti-cyclin A antibody (BF683; Upstate Biotechnology, Lake Placid, NY). The second antibody reaction and the final detection procedure were performed using ECL Western blotting detection reagents (Amersham Biosciences) or SuperSignal West Dura Extended Duration Substrate (Pierce Biotechnology, Rockford, IL) according to the manufacturers' guidance. Information of the chemical luminescence was analogically developed onto Hyperfilm (Amersham Biosciences). After scanning of the developed film, the band intensities were calculated by ImageQuant software (Amersham Biosciences). Stripping of the first antibody was performed by incubating the PVDF membrane with Restore Western Blot Stripping Buffer (Pierce Biotechnology) at room temperature for 30 min.

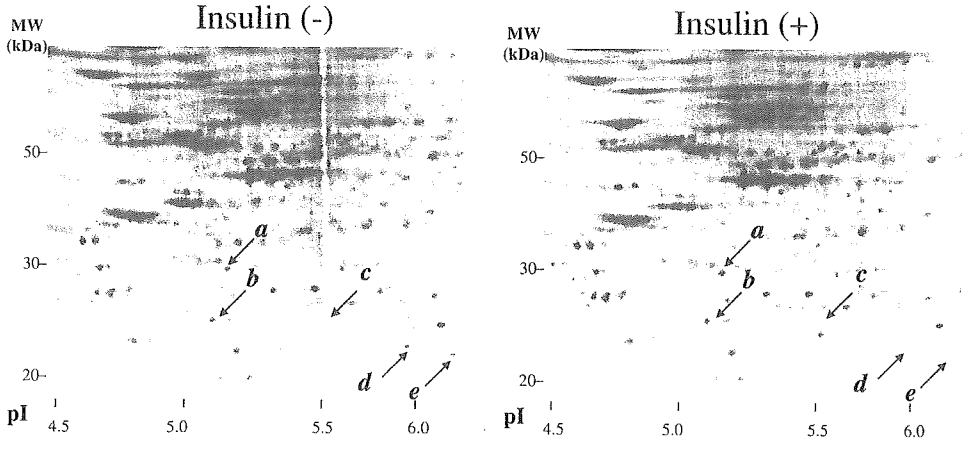

Fig. 1. Two-dimensional electrophoresis (2-DE) profile of human hematopoietic HL-60 cells with or without insulin treatment. HL-60 cells were cultured with transferrin-supplemented serum-free medium for 3 days. Then buffer solution (*left*) or 5 μg/ml insulin (*right*) was added, and cells were cultured for another 1 h at 37°C. Cell lysates were prepared as described in Experimental Procedures, and 2-DE was carried out. PDQuest software-based analysis demonstrated that the 5 spots (indicated by arrows) showed significant differences in their expressions with or without insulin treatment. *Spot a,* CLIC1, an intracellular chloride ion channel; *spot b,* Rho-guanine nucleotide dissociation inhibitor 2 (Rho-GDI-1); *spot c,* and glutathione *S*-transferase-pi (GST-pi); *spots d* and *e,* SRp-20, a splicing factor; *isoform of β-actin.

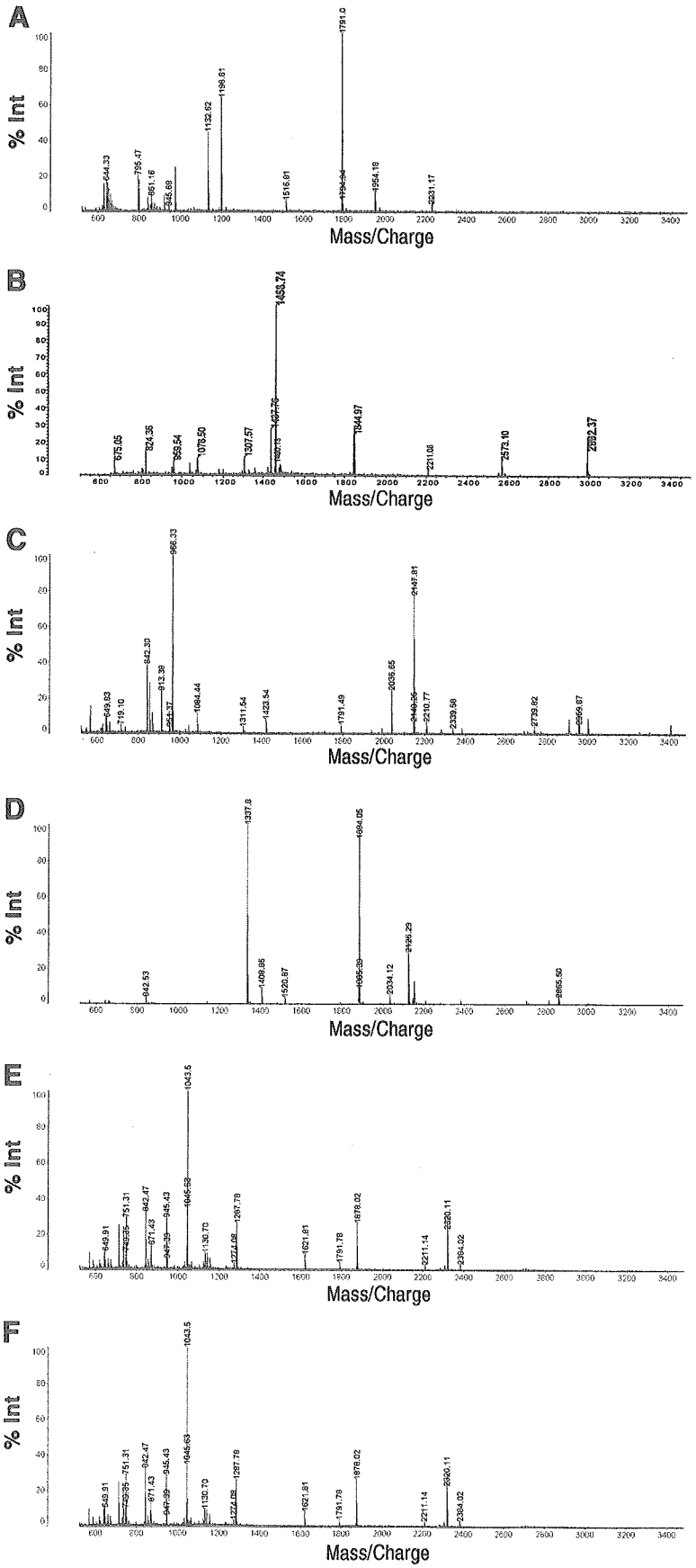

Fig. 2. Peptide mass fingerprinting (PMF) of *spots a–e*. *Spots a* (*B*), *b* (*C*), *c* (*D*), *d* (*E*), *e* (*F*) were picked, and, after trypsin digestion, matrix-assisted laser desorption ionization coupled to a time-of-flight mass spectrometer (MALDI-TOF-MS) analysis was performed. As a positive control, a β-actin spot (* in Fig. 1) was picked and analyzed (*A*).

Two-dimensional Western blotting. SYPRO Ruby-stained proteins on gels were resolubilized and transferred according to our previously reported method (23). Briefly, the stained gel was incubated in resolubilization buffer (0.2% wt/vol SDS, 0.3% wt/vol Tris, 0.7% wt/vol glycine) for 10 min and mounted onto a PVDF membrane in a semidry blotting apparatus (Bio-Rad Laboratories). Electrotransfer was carried out at 4 V/cm^2 for 1 h at room temperature using buffer containing 0.3% (wt/vol) Tris, 1.5% (wt/vol) glycine, 0.1% (wt/vol) SDS. The florescence images of the blotted PVDF membranes were scanned and recorded by FluorImager 595 (Amersham Biosciences). The PVDF membranes were further subjected to immunoblotting as in cases of 1-DE Western blotting.

Cell cycle analysis. Cells (5×10^5) were collected, washed with PBS, and fixed with 70% ice-cold ethanol for 4 h. After treatment with RNase A (100 μg/ml, Sigma) for 30 min at 37°C, DNA was stained with 50 μg/ml propidium iodide (Sigma). Cell cycle analysis was performed by FACScalibur (Becton-Dickinson, Mountain View, CA) using CELL Quest software according to the manufacturer's guidance.

Immunocytochemistry. Cells were fixed on slide glasses with a cytospin apparatus (Cytospin2; Shandon, Pittsburgh, PA) with further fixation with acetone-methanol solution (1:3). The immunostaining procedure was performed as described elsewhere (16) using anti-CLIC1 antibody (1:1,000 dilution) (24). The cells were observed by fluorescent microscopy with Normarsky differentiated interference contrast (Olympus Optical, Tokyo, Japan).

Statistical analysis. Student's *t*-test was used to determine statistical significance. A P value of <0.05 was considered significant.

RESULTS

2-DE protein expression profiles of human hematopoietic cells with or without insulin treatment. To identify novel downstream effectors in early phases of insulin-dependent signals in human hematopoietic cells, we performed the 2-DE-based differential protein expression analysis using human myeloblastic HL-60 cells. The cells which had been cultured in the absence of insulin for 3 days were treated with 5 μg/ml insulin or water. After 1 h, cell lysates were prepared according to the standard isoelectric focusing electrophoresis method described in MATERIALS AND METHODS. In this procedure, highly hydrophobic, urea-insoluble proteins were eliminated during the centrifugation step as precipitants, and only the supernatant fractions were used for 2-DE. In preliminary experiments, we used the immobilized pH gradient gel strip with a broad pH range (pH 3–10 nonlinear) for one-dimensional isoelectric focusing. Although more than 1,000 protein spots were visualized after SYPRO Ruby staining, PDQuest software-based analysis indicated that the spots having significant expression changes by insulin treatment were mainly located at pH 4–6 in the horizontal axis (data not shown). Thus we performed the following detailed analysis using the immobilized pH gradient gel strip with a narrower range (pH 4–7 linear) for finer resolution (Fig. 1). Over 600 protein spots were visualized by SYPRO Ruby staining. From these spots, we selected the candidates for the subsequent mass spectrometric analysis according to the following criteria. The basal expression level was higher than 5% of that of the largest β-actin spot, and the increase or decrease in the expression after insulin stimulation was greater than twofold or less than one-half, respectively. After statistical analysis of the multiple experiments (n = 3–6), five candidates were determined (Fig. 1). These spots were picked from the gel and, after trypsin digestions, MALDI-TOF-MS analysis was performed. Figure 2 shows the PMF of each spot, with a PMF of β-actin as a positive control. These data were further analyzed, being sent to the Mascot search server, and it was suggested that *spot a* was CLIC1, *spot b* was Rho-GDI-2, *spot c* was glutathione *S*-transferase-pi (GST-pi), and *spots d* and *e* were SRp20 (Fig. 2 and Table 1). The Mascot score of each search result was 175 (*spot a*), 80 (*spot b*), 98 (*spot c*), 100 (*spot d*), and 64 (*spot e*), indicating that the protein identifications by PMF were highly reliable (the data are summarized in Table 1). The results of the statistical analysis for the expression amounts of these spots are summarized in Table 2. Among these spots, Rho-GDI-2 (*spot b*) and GST-pi (*spot c*) have already been identified as downstream effectors of insulin. Rho-GDI-2 is reportedly released from the intracellular membrane fractions to the cytoplasm by insulin (19), and the expression of GST-pi markedly increases after insulin stimulation (6). Thus we focused our research on the evaluation of *spot a* and *spots d* and *e*.

To confirm the Mascot search results, we performed 2-DE western blotting by transferring SYPRO Ruby-stained 2-DE protein spots to PVDF membrane. As shown in Fig. 3*A*, most of the proteins were properly transferred to the membrane with a SYPRO Ruby pattern similar to that of the original gel. As shown in Fig. 3*B*, *spot a* was indeed recognized by anti-CLIC1

Table 2. *Ratios of spot intensities (insulin+/insulin−)*

Spot	Protein	Means ± SD	*P* Value
a	CLIC1	1.83±0.37	<0.01
b	Rho-GDI-2	2.03±0.43	<0.02
c	GST-pi	1.93±0.52	<0.05
d	SRp20	0.24±0.33	<0.01
e	SRp20	0.18±0.27	<0.005

Summarized results from 3–6 independent experiments are shown. Statistical analysis was performed by Student's *t*-test.

Table 1. *Protein identification by mass spectrometry analysis*

Spot	GenBank Acc. No.	Protein Name	Mr		pI		Mascot Score	Peptides		Sequence Coverage, %
			Theo, Da	O bs, kDa	Theo	Obs		Match	Total	
a	O00299	CLIC1	2,7248	29.0	5.09	5.16	175	10	11	47
b	P52566	Rho-GDI-2	2,3031	23.6	5.10	5.08	80	6	9	24
c	P09211	GST-pi	2,3438	22.9	5.44	5.67	98	6	8	48
d	P23152	SRp20	1,9546	21.2	11.64	6.13	100	9	11	43
e	P23152	SRp20	1,9546	20.5	11.64	6.38	100	9	11	43

Values of theoretical isoelectric points (pI) and molecular weights/masses (Mr) were obtained from Mascot search results. Theo, theoretical; Obs, observed; CLIC1, intracellular chloride ion channel; Rho-GDI-2, Rho-guanine nucleotide dissociation inhibitor 2; GST-pi, glutathione-*S*-transferase-pi; SRp20, a splicing factor. Calculations of experimental isoelectric point (pI) and molecular weight (Mr) were based on migration of the protein spot on 2-D gels using PDQuest.

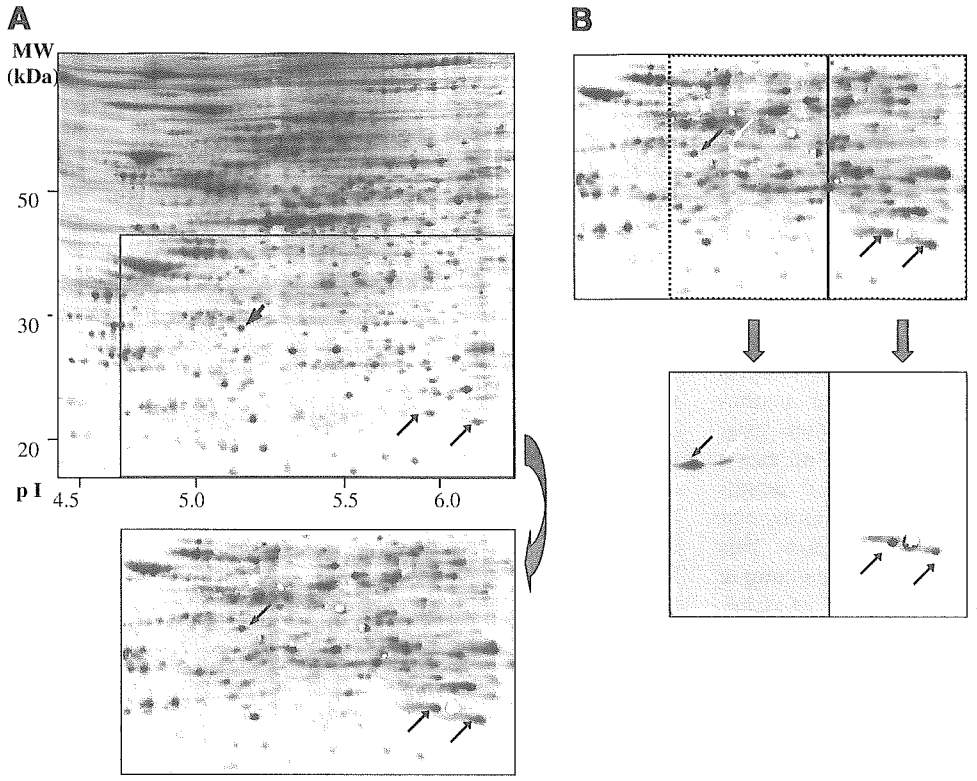

Fig. 3. 2-DE Western blotting. *A*: SYPRO Ruby-stained 2-DE gel, in which the lysate of buffer solution-treated cells were applied as in Fig. 1, *left*, was trimmed (*top*) and transferred onto a PVDF membrane (*bottom*). Transferred proteins were visualized by fluorescence image scanner. *B*: PVDF membrane was cut as indicated and blotted by anti-CLIC1 antiserum (*bottom left*) or anti-SRp20 antiserum (*bottom right*). Spots for CLIC1 and SRp20 are indicated with black arrows. Note that there is an extra spot on the anti-CLIC1-blotted membrane (indicated with white arrow).

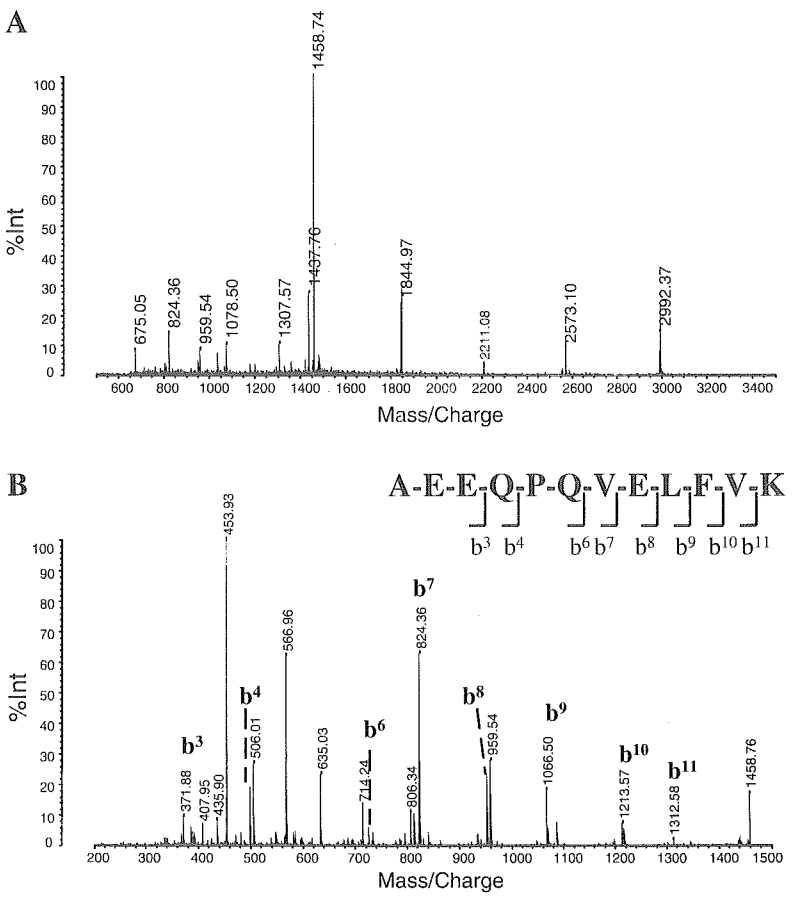

Fig. 4. Amino acid sequencing of NH_2-terminal peptide fragment of CLIC1. Parent ion at *m/z* 1,458.74 in Fig. 2*B* in insulin-treated cells was subjected to subsequent analysis using MS/MS mode of MALDI-TOF-MS (AXIMA-QIT). The mass data of b-series of the product ions were analyzed by the PepSeq program in ProteinLynx software. NH_2-terminal acetylated peptides of *N*-acetyl-AEE (*m/z* 372.14, b^3 ion), *N*-acetyl-AEEQ (*m/z* 500.20, b^4 ion), *N*-acetyl-AEEQPQ (*m/z* 725.30, b^6 ion), *N*-acetyl-AEEQPQV (*m/z* 824.38, b^7 ion), *N*-acetyl-AEEQPQVE (*m/z* 953.42, b^8 ion), *N*-acetyl-AEEQPQVEL (*m/z* 1,066.50, b^9 ion), *N*-acetyl-AEEQPQVELF (*m/z* 1,213.57, b^{10} ion), and *N*-acetyl-AEEQPQVELFV (*m/z* 1,312.64, b^{11} ion) were detected. Peptide mass fingerprinting (PMF; *A*) and MS/MS data of b-series (*B*) are shown. Similar analysis concerning control cells also demonstrated NH_2-terminal acetylation of CLIC1 (data not shown).

antibody and *spots d* and *e* were recognized by anti-SRp20 antibody. We also studied the possible modifications on these two proteins. As shown in Fig. 1*A*, the observed isoelectric point (pI) of CLIC1 was 5.16, which is similar to the Mascot information (the calculated pI was 5.09). Interestingly, there was an extra small spot with a higher pI value (Fig. 3*B*, white arrow). Indeed, we detected a doublet band in one-dimensional Western blotting, where the lysate prepared for 2-DE was mixed with an isovolume of 2× Laemmli's sample buffer and subjected to SDS-PAGE (data not shown and see Fig. 6*B*). Thus CLIC1 is expressed in at least two forms with different pI values in human hematopoietic cells, although the molecular basis for this difference was not elucidated. The MS digest analysis of *spot a* in the 2-DE profiles of both the insulin-treated and control cells demonstrated that the peptide fragment at mass-to-charge ratio (*m/z*) 1,458.74 in PMF of *spot a* represented the NH_2 terminus acetylated fragment acetyl-AEEQPQVELFVK, indicating that the first methionine was eliminated and the second alanine was N-acetylated. This finding was indeed confirmed by the amino acid sequencing at the *m/z* 1,458.74 fragment by the MS/MS mode of MALDI-TOF-MS, as shown in Fig. 4.

As for SRp20, the observed pI values of *spots d* and *e* were 6.13 and 6.38, respectively (Fig. 1 and Table 1), in contrast to the Mascot software information (the calculated pI was 11.64). This discrepancy may come from the modifications of SRp20. The MS digest analysis indicated that the SRp20 was phosphorylated at two sites, including Ser^{115} and Ser^{108}, from the existence of the peptide fragment ions of *m/z* 751.31 and *m/z* 945.43 (Fig. 5*A*). Mass value of *m/z* 751.31 is speculated amino acid sequences as $RRSPR_{(113-117)}$, $RSPRR_{(114-118)}$, or $SPRRR_{(115-119)}$ (Fig. 5*E*). As concerns *m/z* 945.43, MS digest suggests the amino acid sequence as $RRSPPPR_{(106-112)}$, $RSPPPRR_{(107-113)}$, or $SPPPRRR_{(108-114)}$. Phosphorylated peptide was confirmed by MALDI-TOF-MS in a seamless PSD mode (AXIMA-CFR) that detected the neutral loss of phosphate group. As shown in Fig. 5, *B* and *C*, phosphorylation-dependent neutral loss (−80 Da) and dehydration (−18 Da) were detected in the fragments at *m/z* 751.31 and *m/z* 945.43. Conversely, the MALDI-TOF-MS PSD spectrum of the control peptide ion gated at *m/z* 1,043.57 showed no significant neutral loss (Fig. 5*D*). Next, the amino acid sequences of *m/z* 751.31, *m/z* 945.43, and *m/z* 1,043.57 were examined by the same method as described above by using AXIMA-CFRplus. The amino acid sequences of *m/z* 751.31 could not be determined because the fragment ion was low intensity (data not shown). However, it is presumable that the Ser^{115} is phosphorylated. From the mass spectra of gated ion at *m/z* 945.43, the amino acid sequence was determined as $RRSPPPR_{(106-112)}$, and the position of phosphorylation was Ser^{108} (Fig. 6*A*). As a

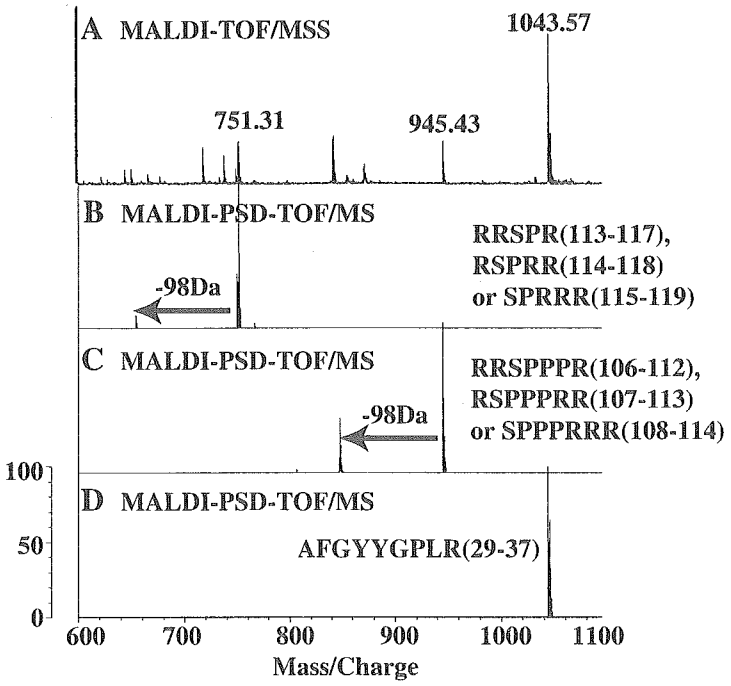

Fig. 5. Confirmation of SRp20 phosphorylation at specific serine residues. *A*: gated ions at *m/z* 751.31, 945.43, and 1,043.57 in Fig. 2*E* were subjected to analysis of neutral loss by MALDI-TOF-MS (AXIMA-CFR) in post-source decay (PSD) mode. The 98-Da loss of mass values was detected in gated ion at *m/z* 751.31 (*B*) and *m/z* 945.43 (*C*), but not in gated ion at *m/z* 1,043.57 (*D*) as a negative control. *E*: primary sequence of SRp20. *Phosphorylated amino acid.

E 1 MHRDSCPLDC KVYVGNLGNN GNKTELERAF GYYGPLRSVW VARNPPGFAF

m/z 1043.57

51 VEFEDPRDAA DAVRELDGRT LCGCRVRVEL SNGEKRSRNR GPPPSWGRRP

101 RDDYRRR*PP PRRRS*PRRRS FSRSRSRSLS RDRRRERSLS RERNHKPSRS

m/z 945.43 *m/z* 751.31

151 FSRSRSRSRS NERK

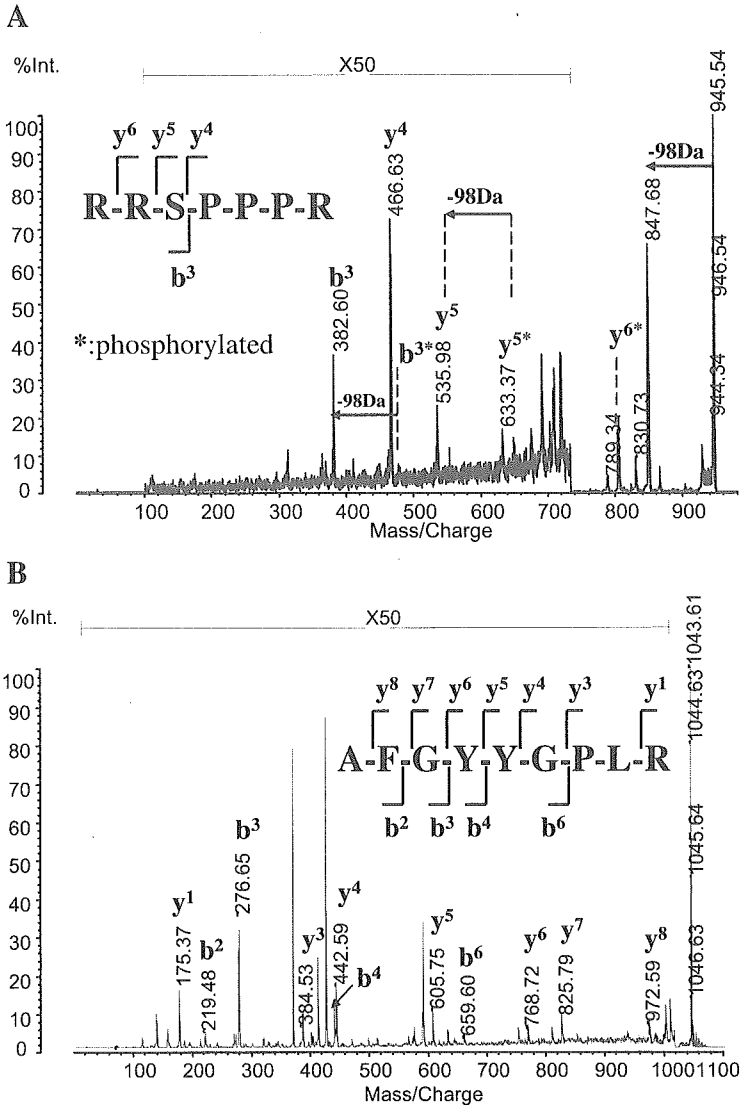

Fig. 6. Sequence analysis of gated ions at *m/z* 945.43 and 1,043.57 by MALDI-TOF-MS in PSD mode. *A*: gated ion at *m/z* 945.29 in Fig. 5*C* was subjected to subsequent analysis using PSD mode of MALDI-TOF-MS (AXIMA-CFRplus) *B*: three neutral loss ions (−98 Da) of *m/z* 480, 633, and 945 were detected. Gated ion at *m/z* 1,043.57 in Fig. 5*D* was subjected to the same analysis. Neutral loss ion (−98 Da) was not detected.

negative control, *m/z* 1,043.57 was subjected to analysis using PSD mode of AXIMA-CFRplus (Fig. 6*B*). The amino acid sequence was decided as AFGYYGPLR$_{(29-37)}$, which was not phosphorylated. These results indicated that Ser^{115} and Ser^{108} were phosphorylated in human hematopoietic cells (Fig. 5*E*). Thus the two phosphorylations of SRp20 may be responsible for the acidic shift of SRp20 in 2-DE.

Thus the 2-DE-based differential protein expression analysis identified CLIC1 and SRp20 as novel downstream effectors of insulin in human myeloblastic HL-60 cells.

1-DE study of CLIC1 and SRp20 expressions after insulin stimulations. It is known that there are occasionally discrepancies between the results of 2-DE and 1-DE. The difference in the protein solubilization capacities between the two systems is thought to be one of the reasons. During cell lysate preparation in 2-DE, highly hydrophobic proteins are prone to make precipitations and thus be eliminated from the lysates after centrifugation. Thus the protein expression changes in 2-DE-based proteome analysis not only means that the net protein expression changes but also the changes in protein solubilization. So we studied the expressions of CLIC1 and SRp20 after insulin stimulation by 1-DE Western blotting.

In contrast to the results of 2-DE, there was no significant difference in CLIC1 expression between insulin-treated and nontreated samples in 1-DE (Fig. 7*A*). Moreover, CLIC1 was detected as a single band, unlike the 2-DE results, where CLIC1 was detected as two spots. Interestingly, CLIC1 was detected as a doublet band, and the expression amounts of CLIC1 were indeed upregulated by insulin stimulation when the 2-DE lysates were treated by an isovolume of 2× Laemmli's buffer and subjected to 1-DE (Fig. 7*B, lane 2*). These findings strongly suggest that insulin treatment induced certain qualitative changes of CLICL1. Compared with 1-DE, the protein recovery rate in 2-DE was generally low: one-fourth the recovery as for CLICI (Fig. 7*B*, compare *lanes 1* and *3*) and one-eighth the recovery as for β-tubulin (Fig. 7*B*, compare *lanes 1* and *3*). However, the expression amounts of β-tubulin (Fig. 7*B*, compare *lanes 1* and *2*) and α-tubulin (data not shown) were not significantly changed by insulin treatment even in 2-DE lysates. By contrast, around a twofold increment in CLIC1 was reproducibly observed after insulin stimulation (Fig. 7, *B* and *C*, and data not shown). We then examined the possibility that the insulin-mediated increments in CLIC1 in 2-DE lysate were associated with the changes in its subcellular

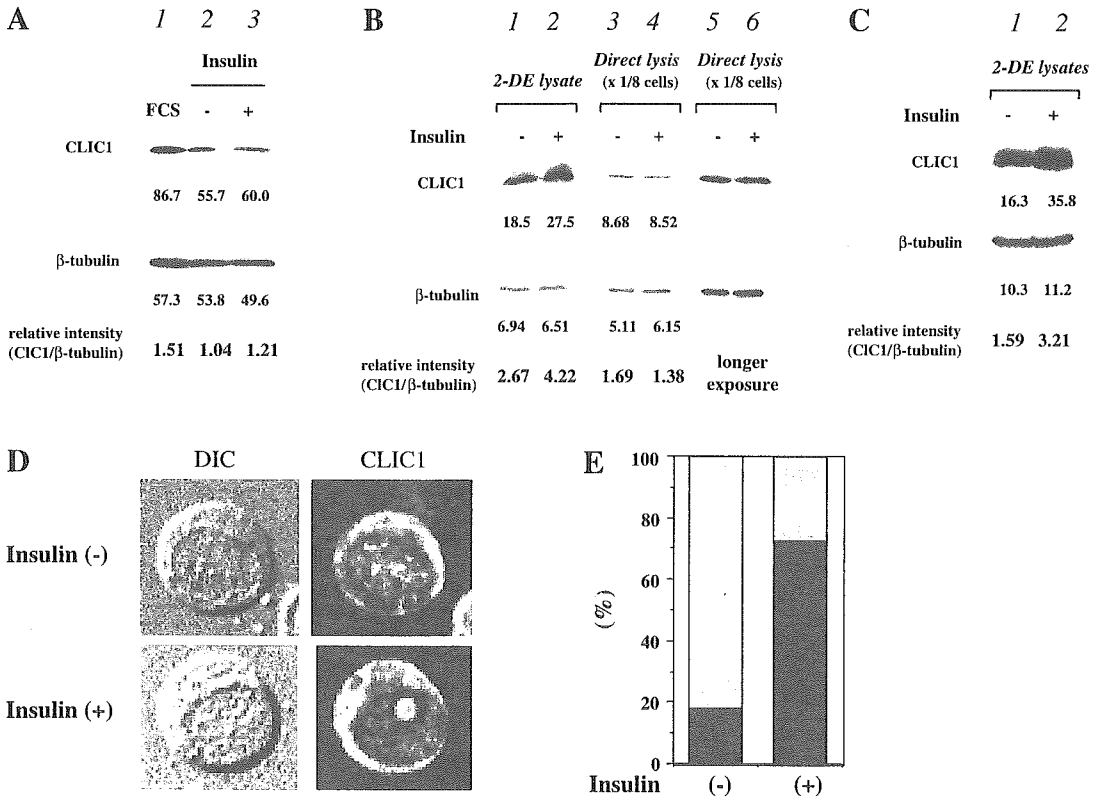

Fig. 7. 1-DE Western blotting of CLIC1. Cells that had been cultured with transferrin-supplemented serum-free medium for 3 days were stimulated by buffer solution (*lane 2*) or insulin (*lane 3*) and incubated for another 1 h at 37°C. *A*: cells were directly lysed with 1× Laemmli's sample buffer and subjected to 1-DE. Western blotting was performed using anti-CLIC1 antiserum. The lysate of the cells that had been cultured in the presence of FCS was also subjected to 1-DE (*lane 1*). Numeral under each band indicates intensity of the protein band. After the first antibody was stripped, the PVDF membrane was reblotted with anti-β-tubulin antibody. *B*: cell lysates prepared according to 2-DE protocol were mixed with isovolume of 2× Laemmli's sample buffer (*lanes 1* and *2*). One-eighth of the cells were directly lysed with 1× Laemmli's sample buffer and subjected to 1-DE (*lanes 3* and *4*). Longer exposure results of *lanes 3* and *4* are shown in *lanes 5* and *6*, respectively. *C*: results of independently performed experiment from *B* are shown. *D* and *E*: subcellular localization of CLIC1. *D*: insulin-treated or nontreated HL-60 cells were stained with anti-CLIC1 antibody. DIC, photograph with Normarsky differentiated interference contrast. *E*: percentages of cells with nuclear speckled staining pattern (filled bars) and cells with nucleoli-staining pattern (gray bars) are shown.

localization. As shown in Fig. 7, *D* and *E*, the nuclear localization pattern of CLIC1 was clearly changed by insulin treatment: CLIC1 was detected mainly as speckled forms in nuclear matrix in nontreated cells, whereas CLIC1 was located mainly at nucleoli in insulin-treated cells. Thus the changes in subnuclear localization may responsible for the expressional changes of CLIC1 in 2-DE.

Next, we studied the expression of SRp20 in 1-DE Western blotting. The SRp20 expression was actually reduced as in the case of 2-DE (Fig. 8*A*), indicating that the total amount of SRp20 was reduced by insulin treatment. To further investigate the molecular basis of insulin-mediated reduction in SRp20, the effects of the proteasome inhibitor MG-132 were examined. As shown in Fig. 8*B*, MG-132 inhibited the insulin-mediated reduction of SRp20 in a dose-dependent manner. MG-132 also blocked the degradation of cyclin D3 and enhanced the accumulation of cyclin D3 after insulin stimulation (Fig. 8*B*, *lane 5*). Interestingly, the recovery of SRp20 expres-

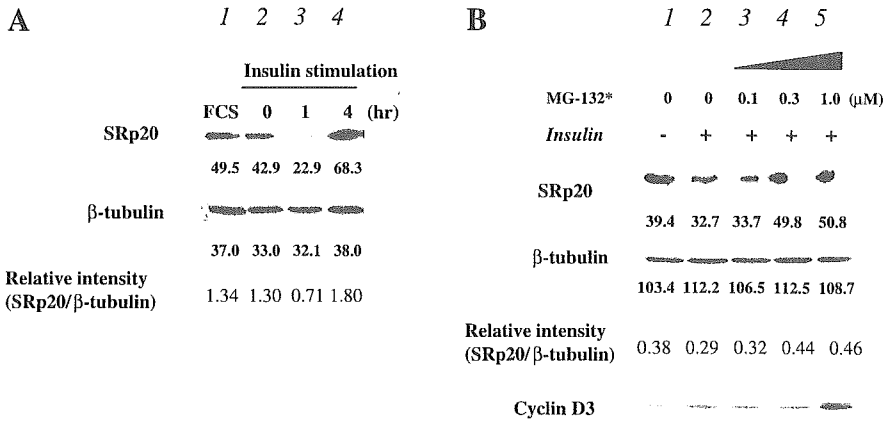

Fig. 8. 1-DE Western blotting of SRp20. Cells were cultured with transferrin-supplemented serum-free medium for 3 days. *A*: cells were then stimulated with insulin, and cell lysates were prepared at indicated times (*lanes 2–4*). Western blotting was performed using anti-SRp20 antiserum. The lysate of cells cultured in the presence of FCS was also subjected to 1-DE (*lane 1*). Numeral under each band indicates intensity of protein band. After the first antibody was stripped, PVDF membrane was reblotted with anti-β-tubulin antibody. *B*: DMSO or increasing doses of MG-132 were added 30 min before insulin stimulation. Cell lysates were prepared 1 h after stimulation and subjected to 1-DE. Western blotting was performed using anti-SRp20 antiserum. PVDF membrane was reblotted with anti-β-tubulin antibody and further with cyclin D3 antibody.

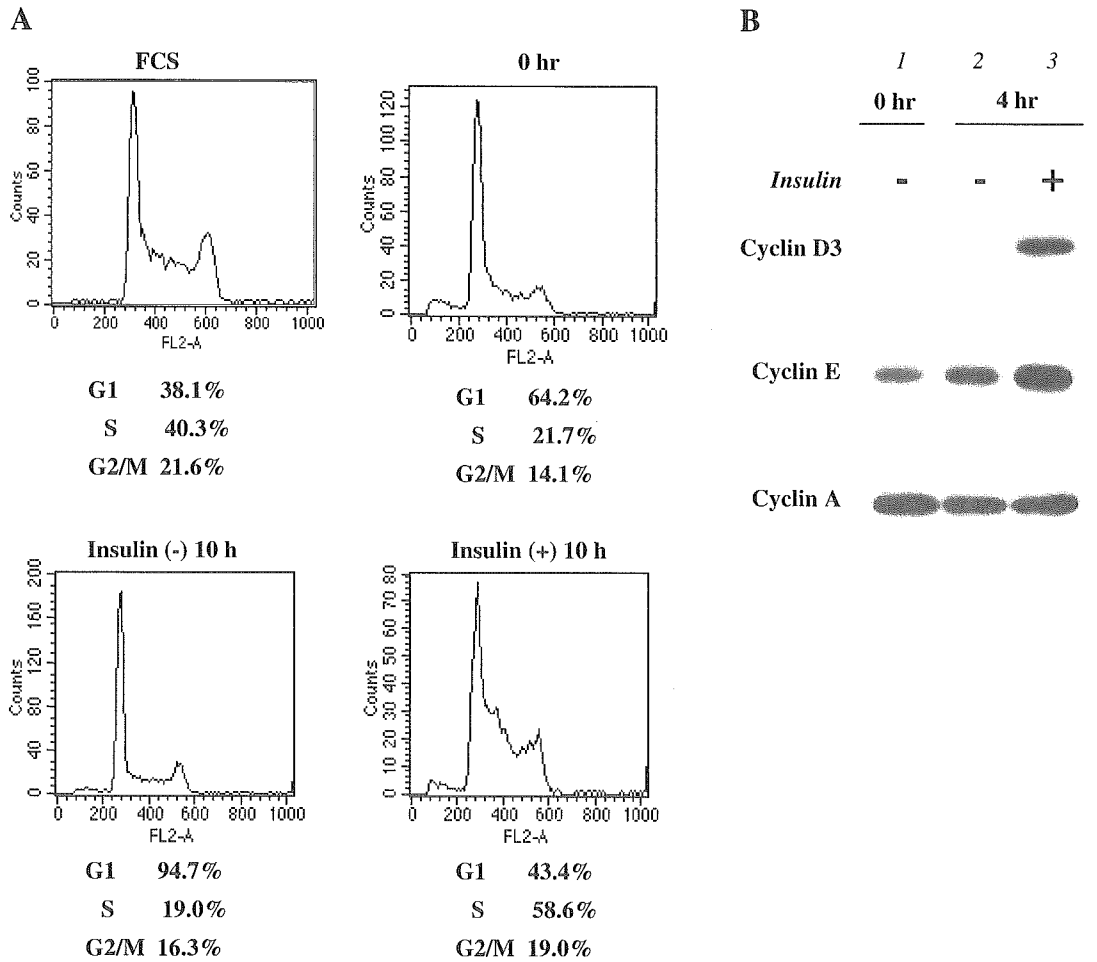

Fig. 9. Cell cycle analysis and expressions of cyclins. *A*: cells cultured with transferrin-supplemented serum-free medium for 3 days were stimulated with buffer solution (*bottom left*) or insulin (*bottom right*). After another 10-h incubation at 37°C, cells were fixed with 70% ethanol and subjected to DNA content assessment by fluorescence-activated cell sorting. Cells cultured in the presence of serum were also subjected to flow cytometric analysis (*top left*). *B*: cells cultured with transferrin-supplemented serum-free medium for 3 days were stimulated with buffer solution (*lane 2*) or insulin (*lane 3*). Cell lysates were prepared after another 4-h incubation. Western blotting was performed using anti-cyclin D3, followed by anti-cyclin E and anti-cyclin A reblotting.

sion was observed 4 h after stimulation (Fig. 8*A*, *lane 4*). Because serum stimulation activates SRp20 transcription and increases the protein expression of SRp20 as the cells enter into S-phase (9), the recovery in SRp2 expression would be associated with the cell cycling progression. As shown in Fig. 9, the insulin treatment significantly increased the S-phased population. Thus the recovery in SRp20 in later phases is associated with an enhanced S-entry.

Thus insulin treatment causes qualitative changes of CLIC1 that are associated with its subnuclear localization and the proteasome-dependent degradations of SRp20 as early as 1 h.

DISCUSSION

We identified CLIC1 and SRp20 as novel downstream effectors of insulin-dependent signals in human hematopoietic cells by using a 2-DE-based proteome analytic system.

A 2-DE-based proteome analysis has merit in managing a wide spectrum of protein expressions atone time. Moreover, it can illustrate the change in modifications and subcellular localization of the proteins besides the change in net amounts. As in the case of CLIC1, glyceraldehyde-3-phosphate dehydrogenase (GAPDH) expressions in 2-DE were upregulated by insulin stimulation, although no significant changes were detected in 1-DE (K. Saeki, unpublished observation). Because serum stimulation, which often induces similar protein expression changes as insulin stimulation, reportedly induces cytoplasmic transport of GAPDH (18), the upregulated expression of GAPDH in 2-DE may be associated with similar subcellular translocation.

Although CLIC1 functions as a chloride ion channel when localized to membranes (26), it is known that CLIC1 localizes principally to the cell nucleus in human hematopoietic cells (24). CLIC1 is structurally homologous to the GST superfamily of proteins with a redox-active site at the NH_2 terminus (5). It is suggested that CLICL1 activity is under the control of redox-active signaling molecules in vivo (5). In this sense, it is interesting that GST-pi is also a downstream effector of insulin as we showed (Fig. 1*A*, *spot c*) and reported elsewhere (6). It is known that hyperglycemia and, to a lesser extent, insulin resistance cause oxidative stress (15, 13). Insulin signaling might possibly contribute to the reduction of oxidative stresses by changing the expression patterns of CLICL1 and GST-pi. Further investigations are required to understand the molecular basis and biological relevance of insulin-induced changes in CLIC1 in the 2-DE system.

As for *spots d* and *e* of SRp20, we could not find any differences in PMFs. One interpretation is that distinct phosphorylations took place at their COOH-terminal SR domains. Because the SR domain is extremely rich in arginine residues, this domain should be degraded into pieces after trypsin digestion, and, as a result, the peptide fragment ions might be hardly detectable. In any case, the expressions of *spots d* and *e* were both decreased by insulin stimulation, and thus the precise determination of structural differences between the two spots would be a less important subject for an understanding of biological effects of insulin. As we showed, the insulin-induced reduction in SRp20 was inhibited by pretreatment of the cells by MG-132, a reversible proteasome inhibitor (Fig. 8*B*). Quite unexpectedly, lactacystin, an irreversible proteasome inhibitor, could not inhibit the reduction of SRp20, although it effectively enhanced an insulin-dependent accumulation of cyclin D3 (K. Saeki, unpublished observation), suggesting that there might be at least two different proteasome-dependent protein degradation systems with distinct lactacystin susceptibilities.

What is the impact of SRp20 reduction by insulin? SRp20 is a splicing factor involved in the regulation of alternative splicing of certain precursor RNA, including SRp20 itself. Its roles for embryogenesis have been shown: an inactivation of SRp20 gene in mice resulted in a failure to form blastocysts, and embryos died at morula stage (11). Although complete loss of SRp20 functions is toxic, its mild reduction may play roles in particular situations. It is reported that overexpression of ASF/SF2, an alternative splicing regulator that antagonizes the function of SRp20 (10), was detected in malignant ovarian tissues (4). A transient reduction of SRp20 by insulin might upregulate the activity of ASF/SF2 and thus trigger signals for cell proliferation. Further investigations are required to determine the in vivo significance of a transient reduction of SRp20 after insulin stimulation.

ACKNOWLEDGMENTS

We greatly thank Masaki Yamada and Tsutomu Nishine of Shimadzu Corporation for technical assistance with the amino acid sequence analysis performed using an MS/MS and PSD mode of MALDI-TOF-MS (AXIMA-QIT and AXIMA-CFRplus).

GRANTS

This work was supported, in part, by a grant for diabetes research (MF-4) from the Organization for Pharmaceutical Safety and Research (to Y. Kaburagi).

REFERENCES

1. **Araki E, Lipes MA, Patti ME, Bruning JC, Haag B III, Johnson RS, and Kahn CR.** Alternative pathway of insulin signalling in mice with targeted disruption of the IRS-1 gene. *Nature* 372: 186–190, 1994.
2. **Blommaart EF, Luiken JJ, Blommaart PJ, van Woerkom GM, and Meijer AJ.** Phosphorylation of ribosomal protein S6 is inhibitory for autophagy in isolated rat hepatocytes. *J Biol Chem* 270: 2320–2326, 1995.
3. **Edvardsson U, Alexandersson M, Brockenhuus von Lowenhielm H., Nystrom AC, Ljung B, Nilsson F, and Dahllof B.** A proteome analysis of livers from obese (ob/ob) mice treated with the peroxisome proliferator WY14,643. *Electrophoresis* 20: 935–942, 1999.
4. **Fischer DC, Noack K, Runnebaum IB, Watermann DO, Kieback DG, Stamm S, and Stickeler E.** Expression of splicing factors in human ovarian cancer. *Oncol Rep* 11: 1085–1090, 2004.
5. **Harrop SJ, DeMaere MZ, Fairlie WD, Reztsova T, Valenzuela SM, Mazzanti M, Tonini R, Qiu MR, Jankova L, Warton K, Bauskin AR, Wu WM, Pankhurst S, Campbell TJ, Breit SN, and Curmi PM.** Crystal structure of a soluble form of the intracellular chloride ion channel CLIC1 (NCC27) at 1.4-A resolution. *J Biol Chem* 276: 44993–5000, 2001.
6. **Hatayama I, Yamada Y, Tanaka K, Ichihara A, and Sato K.** Induction of glutathione S-transferase P-form in primary cultured rat hepatocytes by epidermal growth factor and insulin. *Jpn J Cancer Res* 82: 807–814, 1991.
7. **Jaleel A and Nair KS.** Identification of multiple proteins whose synthetic rates are enhanced by high amino acid levels in rat hepatocytes. *Am J Physiol Endocrinol Metab* 286: E950–E957, 2004.
8. **Joshi RL, Lamothe B, Cordonnier N, Mesbah K, Monthioux E, Jami J, and Bucchini D.** Targeted disruption of the insulin receptor gene in the mouse results in neonatal lethality. *EMBO J* 15: 1542–1547, 1996.
9. **Jumaa H, Guenet JL, and Nielsen P.** Regulated expression and RNA processing of transcripts from the Srp20 splicing factor gene during the cell cycle. *Mol Cell Biol* 17: 3116–3124, 1997.
10. **Jumaa H and Nielsen PJ.** The splicing factor SRp20 modifies splicing of its own mRNA and ASF/SF2 antagonizes this regulation. *EMBO J* 16: 5077–5085, 1997.
11. **Jumaa H, Wei G, and Nielsen PJ.** Blastocyst formation is blocked in mouse embryos lacking the splicing factor SRp20. *Curr Biol* 9: 899–902, 1999.
12. **Kaburagi Y, Yamauchi T, Yamamoto-Honda R, Ueki K, Tobe K, Akanuma Y, Yazaki Y, and Kadowaki T.** The mechanism of insulin-induced signal transduction mediated by the insulin receptor substrate family. *Endocr J* 46, *Suppl*: S25–S34, 1999.
13. **King GL and Loeken MR.** Hyperglycemia-induced oxidative stress in diabetic complications. *Histochem Cell Biol* 122: 333–338, 2004.
14. **Liu JP, Baker J, Perkins AS, Robertson EJ, and Efstratiadis A.** Mice carrying null mutations of the genes encoding insulin-like growth factor I (Igf-1) and type 1 IGF receptor (Igf1r). *Cell* 75: 59–72, 1993.
15. **Robertson RP.** Chronic oxidative stress as a central mechanism for glucose toxicity in pancreatic islet beta cells in diabetes. *J Biol Chem* 279: 42351–42354, 2004.
16. **Saeki K, Hong Z, Nakatsu M, Yoshimori T, Kabeya Y, Yamamoto A, Kaburagi Y, and Yuo A.** Insulin-dependent signaling regulates azurophil granule-selective macroautophagy in human myeloblastic cells. *J Leukoc Biol* 74: 1108–1116, 2003.
17. **Sasaoka T and Kobayashi M.** The functional significance of Shc in insulin signaling as a substrate of the insulin receptor. *Endocr J* 47: 373–381, 2000.
18. **Schmitz HD.** Reversible nuclear translocation of glyceraldehyde-3-phosphate dehydrogenase upon serum depletion. *Eur J Cell Biol* 80: 419–427, 2001.
19. **Shisheva A, Buxton J, and Czech MP.** Differential intracellular localizations of GDP dissociation inhibitor isoforms. Insulin-dependent redistribution of GDP dissociation inhibitor-2 in 3T3-L1 adipocytes. *J Biol Chem* 269: 23865–32868, 1994.
20. **Sun XJ, Rothenberg P, Kahn CR, Backer JM, Araki E, Wilden PA, Cahill DA, Goldstein BJ, and White MF.** Structure of the insulin receptor substrate IRS-1 defines a unique signal transduction protein. *Nature* 352: 73–77, 1991.
21. **Sun XJ, Wang LM, Zhang Y, Yenush L, Myers MG Jr, Glasheen E, Lane WS, Pierce JH, and White MF.** Role of IRS-2 in insulin and cytokine signalling. *Nature* 377: 173–177, 1995.
22. **Tobe K, Tamemoto H, Yamauchi T, Aizawa S, Yazaki Y, and Kadowaki T.** Identification of a 190-kDa protein as a novel substrate for the insulin receptor kinase functionally similar to insulin receptor substrate-1. *J Biol Chem* 270: 5698–5701, 1995.
23. **Toda T, Sugimoto M, Omori A, Matsuzaki T, Furuichi Y, and Kimura N.** Proteomic analysis of Epstein-Barr virus-transformed human B-lymphoblastoid cell lines before and after immortalization. *Electrophoresis* 21: 1814–1822, 2000.
24. **Valentinis B, Romano G, Peruzzi F, Morrione A, Prisco M, Soddu S, Cristofanelli B, Sacchi A, and Baserga R.** Growth and differentiation signals by the insulin-like growth factor 1 receptor in hemopoietic cells are mediated through different pathways. *J Biol Chem* 274: 12423–12430, 1999.
25. **Valenzuela SM, Martin DK, Por SB, Robbins JM, Warton K, Bootcov MR, Schofield PR, Campbell TJ, and Breit SN.** Molecular cloning and expression of a chloride ion channel of cell nuclei. *J Biol Chem* 272: 12575–12582, 1997.
26. **Warton K, Tonini R, Fairlie WD, Matthews JM, Valenzuela SM, Qiu MR, Wu WM, Pankhurst S, Bauskin AR, Harrop SJ, Campbell TJ, Curmi PM, Breit SN, and Mazzanti M.** Recombinant CLIC1 (NCC27) assembles in lipid bilayers via a pH-dependent two-state process to form chloride ion channels with identical characteristics to those observed in Chinese hamster ovary cells expressing CLIC1. *J Biol Chem* 277: 26003–26011, 2002.

International Journal of
HEMATOLOGY

Synergistic Effects of Dehydroepiandrosterone and Retinoic Acid on Granulocytic Differentiation of Human Promyelocytic NB4 Cells

Masami Nakatsu, Masaru Doshi, Kumiko Saeki, Akira Yuo

Department of Hematology, Research Institute, International Medical Center of Japan, Tokyo, Japan

Received August 6, 2004; received in revised form September 28, 2004; accepted October 4, 2004

Abstract

We report a novel effect of dehydroepiandrosterone (DHEA) on human granulocyte differentiation: DHEA enhances the all-*trans*-retinoic acid (ATRA)-induced differentiation of promyelocytic NB4 cells. DHEA (100 μM) significantly augmented the respiratory burst activity of NB4 cells treated with 1 nM ATRA, whereas DHEA alone did not induce respiratory burst activity. The protein and message expressions of $p67^{phox}$, the gene for the dose-limiting component of phagocyte NADPH oxidase, were significantly enhanced by the coexistence of DHEA and ATRA. The protein expression of $p47^{phox}$, another component of phagocyte NADPH oxidase, was also up-regulated by DHEA and ATRA. Moreover, the ATRA-induced increment of CCAAT/enhancer-binding protein β (C/EBPβ) and the reciprocal reduction in C/EBPα expression were also potentiated by DHEA. In contrast, the expression of PU.1, a transcription factor reportedly involved in the basal expression of $p67^{phox}$ in monocytic cells, was only slightly up-regulated by DHEA and ATRA. Interestingly, DHEA sulfate (DHEAS), the sulfate ester of DHEA that exists in peripheral blood at a concentration approximately 3 orders of magnitude larger than that of DHEA, did not stimulate the ATRA-induced differentiation of NB4 cells. Thus, DHEA, but not DHEAS, plays important roles in synergy with ATRA during granulocyte differentiation of human promyelocytic NB4 cells.

Int J Hematol. 2005;81:32-38. doi: 10.1532/IJH97.04117

Key words: DHEA; Granulocytic differentiation; NB4 cells; All-*trans*-retinoic acid; Respiratory burst activity

1. Introduction

Among the various steroid hormones, dehydroepiandrosterone (DHEA) and dehydroepiandrosterone sulfate (DHEAS) are unique in that only the adrenal glands of humans and a few higher primates can synthesize and secrete these hormones in large amounts (reviewed in [1]). Because the plasma concentrations of DHEA and DHEAS steadily decrease with age, DHEA/DHEAS have been considered antiaging hormones (reviewed in [2]). Actually, supplementation with DHEA or DHEAS shows the benefit of preventing lifestyle-related diseases, including obesity, diabetes, and coronary heart disease (reviewed in [3]).

Although free steroids are highly insoluble in water, they become water soluble when conjugated with sulfate. The sulfate ester forms of steroid hormones, however, cannot bind to their nuclear receptors. They become activated only after they are desulfated by steroid sulfatase [4]. Because steroid sulfatase is ubiquitously present in mammalian tissues, it is sometimes difficult to distinguish the in vivo effects of DHEA and DHEAS. Nevertheless, in vitro experiments have shown a clear discrepancy between the effects of DHEA and DHEAS. DHEA, but not DHEAS, inhibits preadipocyte growth and differentiation [5]. In contrast, DHEAS, but not DHEA, stimulates peroxisome proliferator-activated receptor α–induced gene expression [6]. These steroid hormones sometimes show opposite effects. For example, DHEA decreases, but DHEAS increases, the apoptosis of neural precursors from the rat embryonic brain [7]. On the other hand, both DHEA and DHEAS show similar anti-inflammatory effects [8].

Despite the variety of beneficial effects of DHEA/DHEAS, the molecular bases of their effects are largely unknown. Although DHEA reportedly acts as a weak agonist of the pregnane X receptor [9], whether another high-affinity receptor exists remains elusive. Moreover, DHEA and DHEAS can also function as modulators of

Correspondence and reprint requests: Akira Yuo, MD, PhD, Department of Hematology, Research Institute, International Medical Center of Japan, 1-21-1, Toyama, Shinjuku-ku, Tokyo 162-8655, Japan; 81-3-3202-7181; fax: 81-3-3207-1038 (e-mail: yuoakira@ri.imcj.go.jp).

intracellular signal transduction. For example, these hormones can scavenge reactive oxygen species and inhibit nuclear factor κB (NF-κB) activity, resulting in a suppression of inflammation [8].

Although rodent steroidogenic glands, including the adrenals, do not secrete significant amounts of DHEA, possible de novo synthesis of DHEA/DHEAS in the rat brain has been reported [10,11]. DHEA and DHEAS have also been reported to act as neuroactive neurosteroids in the brain by promoting the proliferation and differentiation of neurons [10], protecting apoptosis [12], and even stimulating apoptosis [7]. However, the roles of DHEA/DHEAS in the hematopoietic system are poorly understood. DHEA reportedly ameliorated granulopenia after whole-body γ irradiation in mice [13]. On the other hand, DHEA was shown to inhibit natural killer cell generation and lymphopoiesis but not myelopoiesis in lethally irradiated mice [14]. Apart from the inferences from the studies with these animal models, however, the roles of DHEA/DHEAS in human myelopoiesis have not been studied so far.

We report our study of the effects of DHEA and DHEAS on NB4 cells, undertaken to obtain some insights into the effects of these steroid hormones on human myeloid differentiation. Our results show that DHEA, but not DHEAS, enhances the differentiation of human promyelocytic NB4 cells in combination with a low dose of all-*trans*-retinoic acid (ATRA). The molecular mechanism of DHEA action is also discussed.

2. Materials and Methods

2.1. Cells and Reagents

Human promyelocytic NB4 cells were maintained in RPMI 1640 medium (Life Technologies, Grand Island, NY, USA) supplemented with 10% heat-inactivated fetal bovine serum (JRH Biosciences, Lenexa, KS, USA). DHEA, DHEAS, and ATRA (all from Sigma Chemical Company, St. Louis, MO, USA) were dissolved in solvent solution (90% ethanol and 10% dimethyl sulfoxide [DMSO]), water, and 100% ethanol, respectively. *N*-formyl-methionyl-leucyl-phenylalanine (FMLP) and phorbolmyristate acetate (PMA) (Sigma Chemical Company) were dissolved in DMSO.

2.2. DNA Fragmentation Assay for Apoptosis Detection

The DNA fragmentation assay was performed as described [15]. Cells (3×10^6) were lysed with 350 μL lysis buffer (5 mM Tris, pH 8.0, 0.5% Triton X-100, and 10 mM EDTA). Cell lysates were centrifuged at 15,000 rpm at room temperature for 20 minutes, and the supernatant was treated with 1 mg/mL of heat-inactivated ribonuclease A (Sigma Chemical Company) at 42°C for 60 minutes and with 200 μg/mL proteinase K (Boehringer Mannheim, Mannheim, Germany) for another 60 minutes. After phenol extraction, phenol/chloroform extraction, and ethanol precipitation, the DNA sample was applied to a 1.5% agarose gel, separated by horizontal electrophoresis, and visualized by staining with 500 ng/mL ethidium bromide. A 100–base pair (bp) ladder marker (Toyobo, Osaka, Japan) was used to evaluate the molecular weights of the fragmented DNA.

2.3. Assessment of Respiratory Burst Activity

Respiratory burst activity was evaluated by quantifying superoxide (O_2^-) release. Superoxide was assayed by the superoxide dismutase–inhibitable reduction of ferricytochrome *c*, and the continuous assay was performed in a Hitachi 556 double-wavelength spectrophotometer (Hitachi, Tokyo, Japan) equipped with a thermostated cuvette holder (37°C), as described previously [16]. The final cell concentration was 1×10^6 cells/mL. The reduction of cytochrome *c* was measured at 550 nm with a reference wavelength of 540 nm, and the time course of cytochrome *c* reduction (absorbance change at 550-540 nm) was followed on the recorder. The amount of superoxide released was calculated from the amount of cytochrome *c* reduced in 5 minutes after the addition of FMLP and from the linear portion of the cytochrome *c*–reduction curve for PMA.

2.4. Western Blotting

Cells (5×10^5) were lysed with 100 μL of 1× Laemmli sample buffer and boiled. Cell lysates were then subjected to electrophoresis on a polyacrylamide gel containing sodium dodecyl sulfate (SDS). After electrophoresis, proteins were transferred from the gel onto a nitrocellulose membrane in a buffer containing 25 mM Tris, 192 mM glycine, and 20% methanol at 2 mA/cm^2 for 2 hours at 4°C. Residual binding sites on the membrane were blocked by incubating the membrane for 1 hour at 25°C in Tris buffer (150 mM Tris-HCl, pH 7.6) containing 3% bovine serum albumin. After washing, the membranes were incubated with antibodies to $p67^{phox}$, $p47^{phox}$, CCAAT/enhancer-binding protein α (C/EBPα), C/EBPβ, PU.1 (Santa Cruz Biotechnology, Santa Cruz, CA, USA), and tubulin-α (Lab Vision, Fremont, CA, USA) for 4 hours at 25°C. The secondary antibody reactions were performed with horseradish peroxidase–conjugated antimouse and antirabbit monoclonal antibodies (Cell Signaling Technology, Beverly, MA, USA) or horseradish peroxidase–conjugated antisheep monoclonal antibody (Chemicon, Temecula, CA, USA). The final detection procedure was performed by using SuperSignal West Dura Extended Duration Substrate (Pierce, Rockford, IL, USA) and exposing Hyperfilm (Amersham Biosciences, Buckinghamshire, UK) as described previously [17].

2.5. Reverse Transcription–Polymerase Chain Reaction

RNA was extracted from 5×10^6 cells with an RNeasy Mini kit (Qiagen, Tokyo, Japan), and complementary DNA was synthesized with a Superscript II kit (Invitrogen, Carlsbad, CA, USA) according to the manufacturer's protocol. The reverse transcriptase–polymerase chain reaction (RT-PCR) procedure was performed with Ex Taq (TaKaRa Shuzo, Shiga, Japan) and a DNA thermal cycler (PJ2000; Perkin-Elmer, Foster City, CA, USA) with 30 cycles of 95°C

for 30 seconds, 55°C for 30 seconds, and 72°C for 30 seconds. The primers used were 5′-TGGAGTGTGTCTGGA AGCAG-3′ and 5′-ATCTCTGGGGTTTTCGGTCT-3′ for $p67^{phox}$ and 5′-CTCTTCCAGCCTTCCTTCCT-3′ and 5′-AGCACTGTGTTGGCGTACAG-3′ for β-actin. The PCR products were separated by agarose gel electrophoresis, and the DNA was visualized by ethidium bromide staining.

2.6. Chromatin Immunoprecipitation Assay

Chromatin immunoprecipitation (ChIP) was performed with histone H3 ChIP assay kits (Upstate Biotechnology, Lake Placid, NY, USA). Cells (1×10^6) were fixed with 1% paraformaldehyde at 37°C for 10 minutes. The cells were sedimented, washed, and lysed with SDS lysis buffer (50 mM Tris-HCl, 1% SDS, 10 mM EDTA, 1 mM phenylmethylsulfonyl fluoride, 1 μg/mL aprotinin, and 1 μg/mL pepstatin A). The lysates were sonicated to reduce DNA lengths to between 200 bp and 1000 bp. The soluble fraction was diluted, precleared with salmon sperm DNA/protein A–agarose, and then incubated with 6 μL of antiserum specific for the acetylated forms of histone H3. Then, immune complexes were precipitated with protein A–agarose. The precipitated DNA was eluted with an elution buffer (0.1 M $NaHCO_3$ containing 1% SDS). The eluted material was incubated at 65°C for 6 hours to reverse the formaldehyde cross-links, and DNA was extracted with phenol and chloroform. Ethanol-precipitated DNA was solubilized in water (equivalent to 1×10^6 cells per 100 μL). Semiquantitative PCR was performed with 3, 1, and 0.3 μL of DNA samples (a 3-fold dilution) with 29 cycles of 94°C for 30 seconds, 55°C for 30 seconds, and 72°C for 1 minute. PCR products were resolved by agarose gel electrophoresis and visualized with ethidium bromide staining. The primers used were 5′-CTTTCAGTGGAGAGGGGATG-3′ and 5′-AAGCCA AAAACAGCCTGAAG-3′ for the $p67^{phox}$ promoter region, 5′-CTTCAGGCTGTTTTTGGCTT-3′ and 5′-CCA TGAGAGAGAAAAGGAAAGAAG-3′ for its 3′ downstream region, and 5′-TAAGACTTGCATGCACATACA TTG-3′ and 5′-ACTGCCAAGACTTTTCTAGCCTTA-3′ for its 5′ upstream region. For the lamin A gene ChIP assay, 5′-GGACCTGCAGGAGCTCAATGATCG-3′ and 5′-CCTTAAACTCCTCACGCACTTTGC-3′ were used as primers.

3. Results

3.1. DHEA Enhances NB4 Differentiation in Cooperation with ATRA

In this study, we used a relatively high dose of DHEA (100 μM) in combination with a low dose of ATRA (1 nM) because the lower concentration of DHEA did not exert any effects on NB4 cells (data not shown). One hundred micromolar DHEA alone induced a slight but significant growth suppression (Figure 1A), as has been described in studies of mouse 3T3-L1 cells (median effective dose, 30 μM) [5] and rat and pig primary stromal-vascular cells [18], suggesting that DHEA exerts a particular effect on NB4 cells. Although 100 μM DHEA has also been reported to induce the death of murine preadipocytic 3T3-L1 cells [5], it did not induce the death of human promyelocytic NB4 cells, as assessed by trypan blue staining (data not shown) and apoptotic DNA-ladder formation (Figure 1B).

In the initial experiment of cellular differentiation, we studied the respiratory burst activity controlled by phagocyte NADPH oxidase, a highly sensitive and specific differentiation marker for granulocyte and monocyte lineages. As shown in Figure 2, DHEA up-regulated respiratory burst activity induced by 1 nM ATRA under both PMA-triggered and FMLP-triggered conditions ($P < .01$), although DHEA alone did not induce respiratory burst activity. Thus, DHEA enhances the differentiation-dependent acquisition of respiratory burst activity in synergy with a low dose of ATRA.

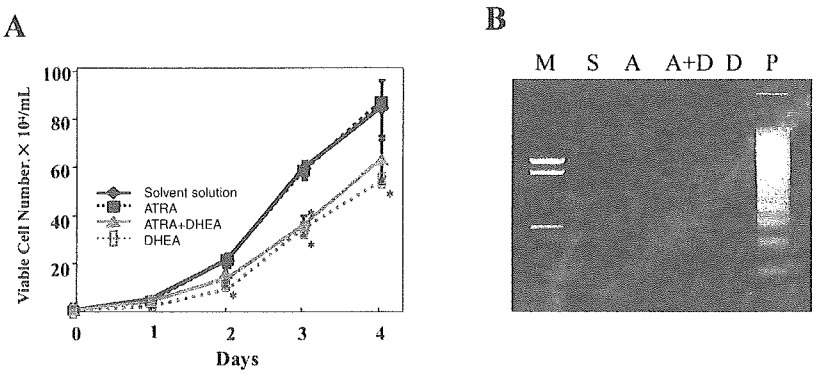

Figure 1. Dehydroepiandrosterone (DHEA) suppresses the growth but does not reduce the viability of NB4 cells. A, Proliferation curve. NB4 cells were treated with solvent solution (final concentrations, 0.09% ethanol and 0.01% dimethyl sulfoxide), 1 nM all-*trans*-retinoic acid (ATRA), 1 nM ATRA plus 100 μM DHEA, or 100 μM DHEA as indicated, and the numbers of viable cells were counted over time. Representative data from 3 independent experiments are shown, and the data are expressed as the mean ± SD of triplicate cultures. B, NB4 cells were treated with solvent solution (S), ATRA (A), ATRA plus DHEA (A+D), or DHEA (D) as indicated. At day 3, low molecular weight DNA was extracted and separated by 1.5% agarose gel electrophoresis. Also indicated as a positive control is the DNA sample from overgrown HL-60 cells (P) [15]. Representative data from 3 independent experiments are shown.

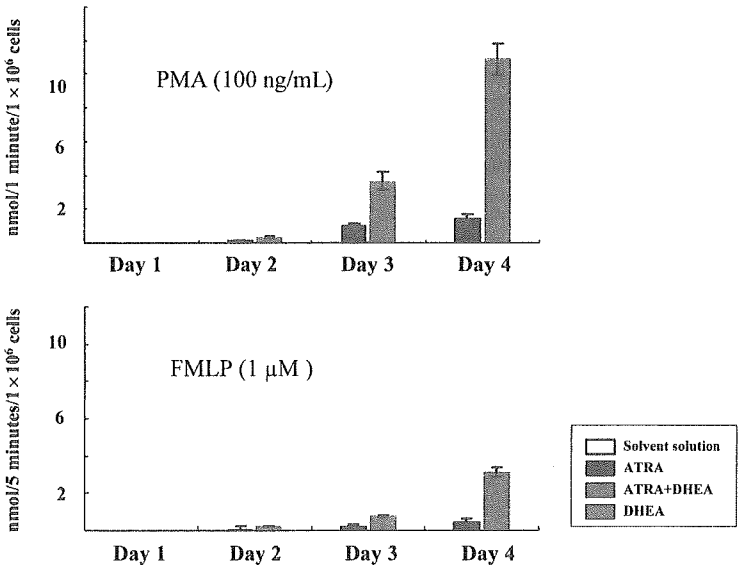

Figure 2. Dehydroepiandrosterone (DHEA) enhances all-*trans*-retinoic acid (ATRA)-induced acquisition of respiratory burst activity. NB4 cells were treated with solvent solution (final concentrations, 0.09% ethanol and 0.01% dimethyl sulfoxide), 1 nM ATRA, 1 nM ATRA plus 100 μM DHEA, or 100 μM DHEA as indicated. Cells were collected over time, and respiratory burst activity was evaluated. Superoxide (O_2^-) release stimulated by 100 ng/mL phorbolmyristate acetate (PMA) (upper panel) and by 1 μM *N*-formyl-methionyl-leucyl-phenylalanine (FMLP) (lower panel) was determined by the reduction of cytochrome *c* and is expressed in nmol/min per 1 × 10^6 cells for PMA and nmol/5 min per 1 × 10^6 cells for FMLP. Representative data from 3 independent experiments are shown, and the data are expressed as the mean ± SD of triplicate cultures.

We then used Western blotting to investigate the expression of the proteins that are involved in or associated with granulocytic differentiation. As shown in Figure 3A, the expression level of $p67^{phox}$, the gene for a dose-limiting component of phagocyte NADPH oxidase [19], was synergistically augmented by DHEA and ATRA, although DHEA alone did not induce $p67^{phox}$ expression. The expression of $p47^{phox}$, the gene for another inducible component of phagocyte NADPH oxidase, was also up-regulated by the presence of both DHEA and ATRA (Figure 3A). The expression of C/EBPβ, a transcription factor that reportedly increases during myeloid differentiation, was indeed enhanced by DHEA and ATRA (Figure 3A). The expression of C/EBPα, which decreases when NB4 cells become differentiated into more

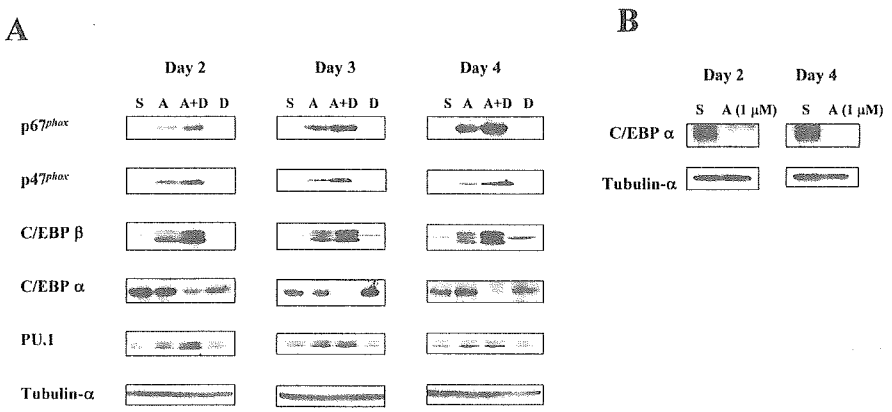

Figure 3. Dehydroepiandrosterone (DHEA) augments all-*trans*-retinoic acid (ATRA)-induced alteration in the expression of differentiation-associated proteins. A, NB4 cells were treated with solvent solution (S) (final concentrations, 0.09% ethanol and 0.01% dimethyl sulfoxide), 1 nM ATRA (A), 1 nM ATRA plus 100 μM DHEA (A+D), or 100 μM DHEA (D) as indicated. Total cell lysates were prepared over time, and Western blotting was performed by using anti-$p67^{phox}$, anti-$p47^{phox}$, anti–C/EBPβ, anti–C/EBPα, anti-PU.1, and anti–tubulin-α antibodies. Representative data from 3 independent experiments are shown. B, NB4 cells were treated with solvent solution (S) (final concentration, 0.1% ethanol) or a high dose of ATRA (A) (1 μM) as indicated. Total cell lysates were prepared at day 2 and day 4, and Western blotting was performed with anti–C/EBPα and anti–tubulin-α antibodies. Representative data from 3 independent experiments are shown.

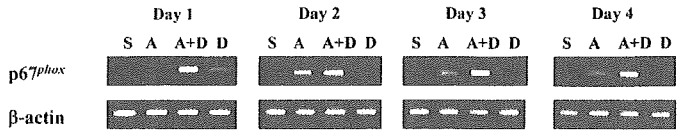

Figure 4. Dehydroepiandrosterone (DHEA) and all-*trans*-retinoic acid (ATRA) synergistically up-regulate p67^{phox} message expression. NB4 cells were treated with solvent solution (S) (final concentrations, 0.09% ethanol and 0.01% dimethyl sulfoxide), 1 nM ATRA (A), 1 nM ATRA plus 100 μM DHEA (A+D), or 100 μM DHEA (D) as indicated. Total RNA was extracted over time, and reverse transcriptase–polymerase chain reaction analyses were performed with p67^{phox}-specific primer pairs (upper panels) or β-actin–specific primer pairs (lower panels). Representative data from 3 independent experiments are shown.

mature stages by a high ATRA dose (Figure 3B), was down-regulated by DHEA and ATRA (Figure 3A). On the other hand, the expression of PU.1, a transcription factor involved in basal p67^{phox} expression in monocytic cells, was only slightly and transiently (only at day 2) up-regulated by the presence of both DHEA and ATRA (Figure 3A).

Thus, a relatively high dose of DHEA and a low dose of ATRA synergistically enhance the differentiation of NB4 cells by augmenting respiratory burst activity, differentiation-dependent p67^{phox} and p47^{phox} induction, differentiation-associated up-regulation of C/EBPβ, and the reciprocal differentiation-associated down-regulation of C/EBPα, without significantly affecting PU.1 expression.

3.2. DHEA Up-regulates p67^{phox} Message Expression without Affecting Histone H3 Acetylation

Because p67^{phox} is the most critical component of phagocyte NADPH oxidase for the acquisition of respiratory burst activity during myeloid differentiation, we focused our study on the molecular mechanism of p67^{phox} induction. First, we used RT-PCR to examine p67^{phox} message expression in the time course after ATRA and DHEA treatment. As shown in Figure 4, the expression of p67^{phoxs} message was synergistically up-regulated by DHEA and ATRA. Two independent experiments gave similar results (data not shown).

Because DHEA is a steroid hormone, it may possibly act as a ligand of a nuclear receptor to enhance transcription. It may also work in the cytoplasm, because DHEA and DHEAS, unlike other steroid hormones, function as cytoplasmic signal transduction modulators. For example, they are reportedly involved in anti-inflammation via the scavenging of reactive oxygen species, thereby inhibiting NF-κB activities [8]. Because sulfate ester forms of steroid hormones cannot bind to nuclear receptors, DHEAS cannot affect NB4 differentiation if DHEA works as a ligand of a nuclear receptor. On the other hand, DHEAS can show an effect similar to that of DHEA if DHEA works in the cytoplasm as a signal transduction modulator.

To address this point, we added DHEAS to NB4 cells along with a low dose of ATRA and evaluated the differentiation-dependent respiratory burst activity. As shown in Figure 5, DHEAS completely failed to enhance the ATRA-induced respiratory burst activity of NB4 cells under the same conditions in which DHEA potently enhanced this activity (Figure 2). Thus, it is highly possible that DHEA functions as a ligand of a particular nuclear receptor.

Steroid hormones play important roles in chromatin remodeling by regulating the corepressor/coactivator-complex exchanges [20]. On binding of steroid hormones to their nuclear receptors, the histone deacetylase–containing corepressor complex is eliminated, and the histone acetyltransferase–containing coactivator complex is recruited to the chromatin, inducing the hyperacetylation of histone H3. Therefore, we used the ChIP assay to examine the histone H3 acetylation state at the p67^{phox} promoter region (corresponding to bp –246 to bp +14 relative to the transcription start site), a 5′ upstream region (corresponding to bp –2261 to bp –1928 relative to the transcription start site), and a 3′ downstream region (corresponding to bp +14 to bp +329 relative to the transcription start site).

As shown in Figure 6, histone H3 acetylation was up-regulated by ATRA treatment by approximately 3-fold in all of these regions. ChIP assays targeting broader regions in the p67^{phox} gene (covering bp –2261 to bp +36,922 relative to the transcription start site) gave similar results (data not shown). Again, DHEA alone did not influence the histone H3 acetylation states. Unexpectedly, DHEA did not enhance ATRA-induced histone H3 acetylation (Figure 6), although it clearly augmented ATRA-induced p67^{phox} message expression (Figure 4). Thus, DHEA up-regulates p67^{phox} message expression without affecting histone H3 acetylation.

4. Discussion

We have shown that DHEA enhances the ATRA-induced differentiation of human promyelocytic NB4 cells. We have demonstrated that DHEA potentiates the ATRA-induced respiratory burst activity via a synergistic up-regulation of p67^{phox} message expression. It also intensifies the ATRA-induced alteration in the expression of proteins such as C/EBPα and C/EBPβ.

The in vivo significance of retinoic acid signaling in myeloid differentiation is rather controversial. In the in vitro colony-formation assay, bone marrow populations of retinoic acid receptor α1/retinoic acid receptor γ double-null mice were blocked at the myelocyte stage and, to a lesser extent, at the metamyelocyte stage. However, the bone marrow cells appear to differentiate normally in vivo, suggesting an effective compensation mechanism in these mice, at least in vivo [21]. An argument against the in vivo significance of ATRA in granulocyte differentiation derives from the fact that the plasma concentration of ATRA is quite low. The ATRA con-

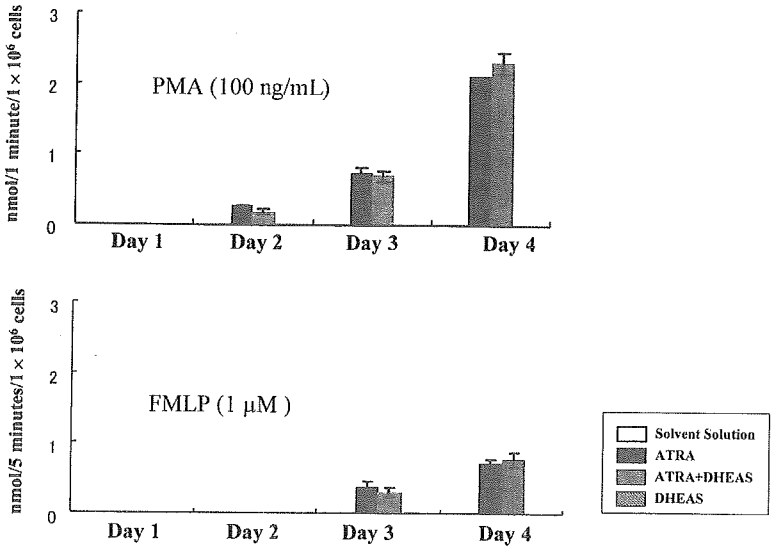

Figure 5. Dehydroepiandrosterone sulfate (DHEAS) does not enhance all-*trans*-retinoic acid (ATRA)-induced respiratory burst activity. NB4 cells were treated with solvent solution (final concentration, 0.09% ethanol), 1 nM ATRA, 1 nM ATRA plus 100 μM DHEAS, or 100 μM DHEAS as indicated. Cells were collected over time, and the respiratory burst activity was evaluated. Superoxide (O_2^-) release stimulated by 100 ng/mL phorbolmyristate acetate (PMA) (upper panel) and by 1 μM *N*-formyl-methionyl-leucyl-phenylalanine (FMLP) (lower panel) was determined by the reduction of cytochrome *c*, and is expressed in nmol/min per 1 × 10^6 cells for PMA and nmol/5 min per 1 × 10^6 cells for FMLP. Representative data from 3 independent experiments are shown, and the data are expressed as the mean ± SD of triplicate cultures.

centration in peripheral blood is approximately 15 nM in healthy individuals, whereas 1 μM ATRA has been used in in vitro differentiation experiments. Certain factors that exist in human plasma but not in fetal bovine serum may work in cooperation with ATRA to make it possible for a low dose of ATRA to induce myeloid differentiation in vivo. Our findings strongly suggest that DHEA, which potentiates the action of a low dose of ATRA (1 nM) and cooperatively induces myeloid differentiation, is one candidate for such a cooperative factor of ATRA. Apart from the in vivo significance of DHEA, it can also provide therapeutic benefits for the treatment of ATRA-resistant promyelocytic leukemia by potentiating the weakened ATRA signaling.

The molecular mechanism of cooperation between DHEA and ATRA during granulocytic differentiation of NB4 cells remains elusive. DHEA has been reported to act as an inhibitor of glucose-6-phosphate dehydrogenase and thus inhibit the PMA-triggered respiratory burst in human neutrophils [22]. In our study, however, DHEA did not inhibit, but rather augmented, PMA-triggered respiratory burst activity in ATRA-treated differentiated NB4 cells. Thus, a completely different mechanism must have been working in our case. DHEA and retinoic acid have also been reported to synergistically promote the differentiation of human neuroblastoma cells [23]. In that case, however, DHEA enhanced neuroblastoma differentiation via signaling that was not mediated by retinoic acid receptor: retinoic acid enhances the activity of matrix metalloproteinase 2, and DHEA enhances the activity of matrix metalloproteinase 9 [23].

In the present study, the effects of ATRA and ATRA plus DHEA were highly analogous, with the ATRA effect becoming amplified under conditions of ATRA plus DHEA with respect to $p67^{phox}$ message expression and protein expression of $p67^{phox}$, $p47^{phox}$, C/EBPα, and C/EBPβ. Thus, DHEA signaling seems likely to have certain interactions with ATRA signaling, at least in NB4 cells. As we have

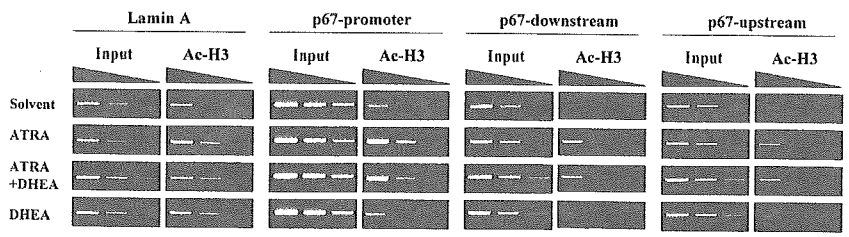

Figure 6. Histone H3 acetylation (Ac-H3) of the $p67^{phox}$ gene during NB4 differentiation. NB4 cells were treated with solvent solution (final concentrations, 0.09% ethanol and 0.01% DMSO), 1 nM all-*trans*-retinoic acid (ATRA), 1 nM ATRA plus 100 μM dehydroepiandrosterone (DHEA), or 100 μM DHEA as indicated. At day 4, cells were collected and the chromatin immunoprecipitation assay was performed with specific primer pairs for the lamin A gene, the $p67^{phox}$ gene promoter region, and its upstream and downstream regions. Representative data from 3 independent experiments are shown.